JIMMA UNIVERSITY

SCHOOL OF GRADUATE STUDIES

JIMMA INSTITUTE OF TECHNOLOGY

FACULITY OF CIVIL AND ENVIRONMENTAL ENGINEERING

STRUCTURAL ENGINEERING STREAM

DEVELOPMENT OF UNIAXIAL INTERACTION DIAGRAM FOR CIRCULAR CONCRETE FILLED STEEL TUBE COLUMNS USING FINITE ELEMENT ANALYSIS

A Thesis Submitted to School of Graduate Studies of Jimma University in Partial Fulfillment of the Requirements for the Degree of Masters of Science in Structural Engineering

By:

NIGIST CHANE

January, 2020

Jimma, Ethiopia

JIMMA UNIVERSITY

SCHOOL OF GRADUATE STUDIES

JIMMA INSTITUTE OF TECHNOLOGY

FACULITY OF CIVIL AND ENVIRONMENTAL ENGINEERING

STRUCTURAL ENGINEERING STREAM

DEVELOPMENT OF UNIAXIAL INTERACTION DIAGRAM FOR CIRCULAR CONCRETE FILLED STEEL TUBE COLUMNS USING FINITE ELEMENT ANALYSIS

A Thesis Submitted to School of Graduate Studies of Jimma University in Partial Fulfillment of the Requirements for the Degree of Masters of Science in Structural Engineering

By: NIGIST CHANE

Advisor: Engr. ELMER C. AGON, Asso. Prof.

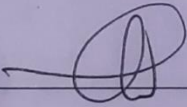Co-Advisor: Engr. YOHANNES WERKINA
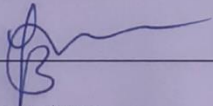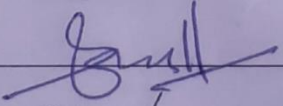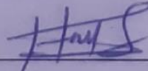
January, 2020

Jimma, Ethiopia

JIMMA UNIVERSITY

SCHOOL OF GRADUATE STUDIES
JIMMA INSTITUTE OF TECHNOLOGY
FACULTY OF CIVIL AND ENVIRONMENTAL ENGINEERING
STRUCTURAL ENGINEERING CHAIR

DEVELOPMENT OFUNIAXIAL INTERACTION DIAGRAM FOR CIRCULAR CONCRETE FILLED STEEL TUBE COLUMN USING FINITE ELEMENT ANALYSIS

NIGIST CHANE

APPROVED BY BOARD OF EXAMINERS

1. Engr. Elmer C. Agon _____ 04 / 02 / 2020

    Main advisor   Signature   Date

2. Engr. Yohannes Werkena _____ 04 / 02 / 2020

    Co-advisor   Signature   Date

3. Dr. S. Moses Aranganathan _____ 31 / 01 / 2020

    External Examiner   Signature   Date

4. Engr. Diosdado John Corpuz _____ 01 / 02 / 2020

    Internal Examiner   Signature   Date

5. Engr. Haymanot G/silassie _____ 04 / 02 / 2020

    Chairperson   Signature   Date

DECLARATION

I declare that this thesis is my original work and has not been presented for a degree in any other university. Wherever contribution of others is involved, every effort is made to indicate this clearly, with due reference to the literatures.

Name: Nigist Chane

Signature:

Date: January, 2020

APPROVED BY:

Engr. Elmer C. Agon, Asso. Prof.
<table>
<tr><td></td><td></td></tr>
</table>

Advisor	Signature	Date

Engr. Yohannes Werkina

Co-Advisor	Signature	Date

ACKNOWLEDGEMENT

ABSTRACT

In recent times, concrete filled steel tubes have gained worldwide acceptance in the construction of high rise and large span structures due to their structural efficiency. Steel tube serves as both reinforcement and formwork, eliminating the need for both, and provides large tensile and compressive capacities. The concrete fill restrains buckling of the steel tube, which increases the strength and stiffness of the section. However, their designs involve tiresome calculations and interaction charts development procedures.

This study involves numerical investigations on the performance of concrete-filled-steel-tube (CFST) finite element models subjected to axial loading. Nonlinear material models for confined concrete and steel tubes were used. The results obtained from the finite element analysis were verified against prior experimental results by comparing its results and axial load-displacement curves. Finally, outputs from the finite element analysis were used to develop uniaxial interaction charts for circular CFST columns. Axial load eccentricity due to lateral mid height deflection of column, P-Δ or second order effect was considered to determine moment capacity.

The study shows confinement of concrete core provided by the steel tube increases strength and ductility of concrete, which considerably maximizes axial load and bending moment capacity of the CFST column by about 25% and 17% respectively. It has been noted that increase in diameter of circular CFSTs enhanced load and moment capacity. It was also observed that eccentric axial loading conditions have notable effects on load resistance of a column. This numerical analysis perceived that column length also have a remarkable effect in which mid height deflections were pronounced by 82% for longer columns. The proposed interaction diagram was compared with that predicted by Eurocode4. The comparison confirms that strength of CFST column computed by EC4 is more conservative.

Keywords*: Circular concrete-filled steel tube columns; N-M interaction curve; Nonlinear finite-element analysis*

TABLE OF CONTENTS

Contents   **Page**

LIST OF FIGURES

LIST OF TABLES

NOTATIONS

Ac	Cross-sectional area of concrete
Acc	Cross-sectional area of concrete under compression
As	Cross-sectional area of steel profile
$CCFST$	Circular concrete filled steel tube
CFT	Concrete filled tube
$CFST$	Concrete filled steel tube
Es	Elastic modulus of steel
Ecm	Secant modulus of the concrete
ε_{c1}	Peak strain
ε_c	Ultimate strain
FEA	Finite element analysis
fck	Characteristic concrete strength
f_{cm}	Mean compressive strength
f_t	Tensile strength
f_{cu}	Cubic concrete strength
f_y	Yield strength of structural steel
f_{cd}, f_{yd}	Design strength for concrete and steel
h_i	Neutral axis distance from centroidal axis

G_f	Fracture energy
$M_{max,Rd}$	Maximum moment resistance
M_u	Bending resistance of the cross-section
N_{cr}	Elastic critical load
N_{Sd}	Axial design loading
$Npl.Rd$	Axial plastic resistance of a cross-section
Npm,rd	Compressive resistance force for the whole area of concrete
N_u	Axial compressive resistance
t	wall thickness of steel tube
v	Normalized Axial compressive resistance
w	Ratio of contribution to overall axial plastic resistance of steel section to concrete section
W	Crack displacement
W_c	Critical crack opening displacement
γ_{M1} , γ_c	Partial safety factors for steel and concrete, respectively
λ	Relative slenderness ratio
μ	Normalized bending resistance of the cross-section
η_s, η_c	Coefficients for considering effect of confinement for circular cross-section
χ	Factor taking account for the influence of imperfection and slenderness

CHAPTER ONE

INTRODUCTION

1.1 Background

Over the last few decades, steel-concrete composite structures have been used widely in modern bridge and high rising building construction. Composite structure integrates the structural and constructional qualities of both steel and concrete. Concrete is good in compression and fire resistance, has low material costs, and easy to place. Steel has high ductility, high strength-to weight and stiffness-to-weight ratios. Combining the advantages of both materials, composite structures will result in cost and time efficient construction. A steel-concrete composite column is conventionally a compression member, in which the steel element is a structural steel section, comprising either a concrete encased or a concrete filled tubular section. In a composite column, both the steel and concrete resist the external loading by interacting together through bond and friction. Concrete filled steel tube (CFST) columns are valuable structural members when compared with separate reinforced concrete columns or steel hollow columns. The steel tube acts as permanent formwork, and provides lateral confinement or lateral reinforcement to the concrete whilst local buckling which is normal a problem with thin-walled steel tube is delayed due to the presence of the concrete infill [1].

The resistance of a concrete filled steel tube column subjected to axial load is determined using P-M interaction curve. Interaction diagram is a curve that shows the possible combination of moment and axial load that will cause failure to a given cross section. In a typical interaction curve of a column with steel section only the moment resistance undergoes a continuous reduction with an increase in the axial load. However, a short composite column will often exhibit an increase in the moment resistance beyond plastic moment under relatively lower values of axial load. This is because the compressive axial load prevents concrete cracking and makes the composite cross-section of a short column more effective in resisting moment [2]. Including EBCS-4 [3] or Eurocode 4 [4] most codes

of practice such as, the widely used AISC-LRFD, ACI-318 have incorporated simplified methods for analysis and design of composite columns. These provisions are generally extrapolated from either reinforced concrete column or steel column design codes.

1.2 Statement of the Problem

In EBCS-EN 1994-1-1: 2013, a simplified method is provided for the analysis and design of composite column. But, this method is applicable for symmetrical sections fulfilling certain requirements. In this method, the moment-axial force interaction curve of a cross-section is determined by assuming full plastic stress distributions. The evaluation of points on the interaction curve this way is computationally difficult. For this reason, the interaction curve is further approximated with a polygon made by computing four or five points of the curve. The capacity of the column is determined using the interaction curve of its cross-section by accounting for the slenderness and member imperfection effects. Finally, the column length is checked whether it is capable of resisting the design action effects or not. If the capacity of the column length turned out to be inadequate or over designed, another section will have to be assumed and the above process is repeated all over again. In addition, a rigorous section analysis is mandatory for all other sections that fail to satisfy the code preconditions.

Even though composite structural system is well practiced advanced construction method worldwide for high rise structures, it is a relatively new concept for the construction industry of Ethiopia. But composite column can be well suited with all its benefits it can accelerate the current large scale infrastructure constructions. Specially steel-concrete composite structure can improve the quality and time delay in the construction of multi-storied and large span buildings and bridges. It is a customary practice for a structural engineer to design reinforced concrete columns regardless of the nature of structures. When increasing the amount of usable floor space in office or other type of buildings is required, smaller column sizes may be used. As a result, an individual column may be subjected to high axial load and moments. In these cases, composite columns provide high strength

applications serving the architectural purpose. However, neither design aid nor analyses tool have not been developed according to the revised Ethiopian building codes yet.

Noticing these gaps and since, construction of a composite cross section interaction curve is time consuming; this thesis makes an attempt to present practical interaction charts for certain dimensions of CFST circular columns which are assumed to be more economical sections.

1.3 Objectives of the Study

1.3.1 General objective

The main objective of this study was to develop uniaxial interaction diagram for circular concrete filled steel tube columns according to the EBCS-EN1994-1-1:2013 using Abaqus/CAE 2017.

1.3.2 Specific objectives

- To check the design procedure of composite columns according to simplified method of EBCS-EN 1994-1-1: 2013.
- To examine the combined effect of axial load and moment over CFST column design and analysis
- To provide interaction curve for a corresponding geometric property, eccentricity and steel ratio of a CFST column.

1.4 Significance of the Study

This research was conducted to develop uniaxial interaction curves for circular concrete infilled steel tubular columns subjected to axial load in particular. These charts predict cross-sectional strength in terms of axial load and moment resistance capacity for CCFST columns. Since uniaxial interaction diagrams predict ultimate capacity, outputs of this study enables to determine the size of circular CFST column to be used in design.

1.5 Scope and Limitation of the Study

The study emphasizes on developing uniaxial interaction chart for circular concrete filled steel tube column with same material strength (concrete and steel grade). The procedure used to study the interaction of axial load and bending moment of circular CFST column was limited to finite element analysis. Experimental or physical tests investigating CFST column behaviors under axial loading were not involved.

CHAPTER TWO

RELATED LITERATURE REVIEW

Steel-Concrete composite structures are nowadays very popular owing to their advantages over conventional Concrete and Steel constructions. Its success is due to the strength and stiffness that can be achieved, with minimum use of materials. Composite construction integrates the best properties of both concrete and steel which results in a highly efficient and lightweight unit that is commonly used for structures such as multi-storey buildings and bridges. Composite column is among the structural composite members. The beginning of frequent use of composite columns in tall buildings dates to about 1980 [5].

Composite columns can have high strength for relatively small cross-sectional area, meaning that several usable floor spaces can be maximized. Concrete can restrain slender steel sections from local or lateral torsional buckling. Both have the same thermal expansion, beside the fact that concrete gives corrosion protection and thermal insulation to the steel at elevated temperature [6].

Beside concrete encased sections, composite columns can also be constructed without the use of formwork, by filling a steel tube with concrete (CFT). A notable early use of filled tubes (1966) was in a four-level motorway interchange [7].

Bond develops either from adhesion between concrete and steel or from friction due to normal stress. The magnitude of friction force developed in CFT column depends on the rigidity of the tube walls against pressure perpendicular to their plane. If the bond is not sufficient to transfer the load between the steel and concrete, provide the top region of the steel tube with mechanical shear connectors to ensure full composite action [6].

In EBCS EN 1994 composite columns and composite compression members in general are categorized as:

- concrete encased sections (a)
- partially encased sections (b, c)
- concrete filled rectangular and circular tubes (d, e & f)
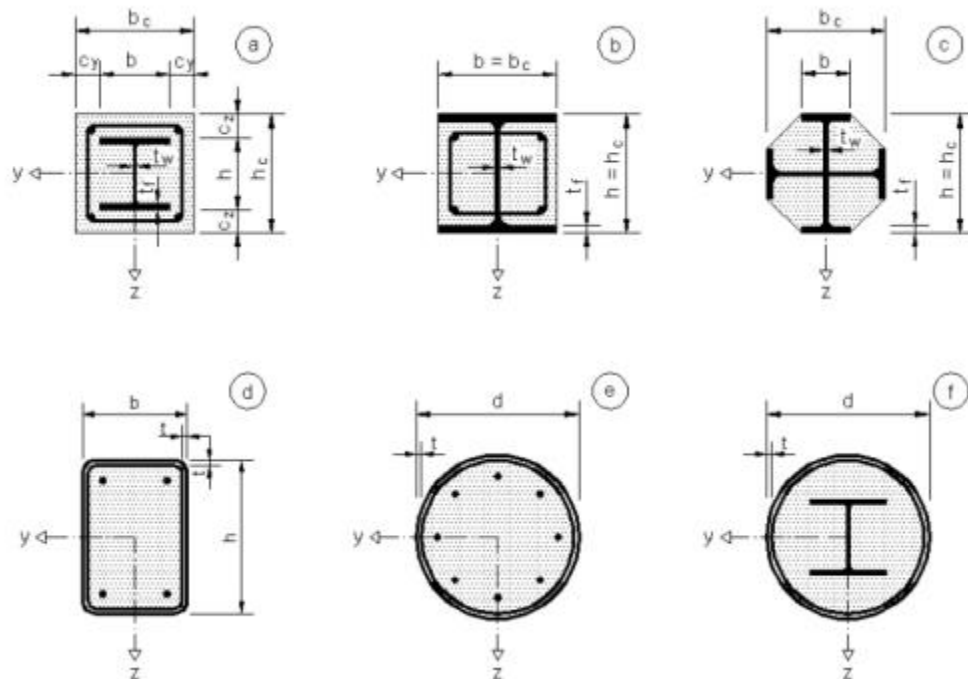
Figure2.1 Typical cross-sections of composite columns and notation [3]

In this research concrete-filled steel tubes (CFT) are going to be considered. Concrete filled steel tubes (CFTs) are composite members consisting of a steel tube in filled with concrete. In current international practice, CFT columns are used in the primary lateral resistance systems of both braced and unbraced building structures. There exist applications in Japan and Europe where CFTs are also used as bridge piers. Moreover, CFTs may be utilized for retrofitting purpose for strengthening concrete columns in earthquake zones [5].

The CFT structural member has a number of distinct advantages over an equivalent steel, reinforced concrete, or steel-reinforced concrete member. The orientation of the steel and

concrete in the cross-section optimizes the strength and stiffness of the section. The steel lies at the outer perimeter where it performs most effectively in tension and resisting bending moment. Also, the stiffness of CFT is greatly enhanced because the steel, which has a much greater modulus of elasticity than the concrete, is situated furthest from the centroid, where it makes the greatest contribution to the moment of inertia [8]. The concrete forms an ideal core to withstand the compressive loading in typical applications, and it delays and often prevents local buckling of the steel particularly in rectangular CFTs. Additionally, it has been shown that the steel tube confines the concrete core, which increases the compressive strength for circular CFTs, and the ductility in rectangular CFTs. Therefore, it is advantageous to use CFTs for columns subjected to large compressive loading. In contrast to reinforced concrete columns with transverse reinforcement, the steel tube also prevents spalling of the concrete and minimizes congestion of reinforcement in the connection region, particularly for seismic design. Numerous tests have illustrated the increase in cyclic strength, ductility and damping by filing hollow tubes with concrete. Recent applications have also introduced use of high strength thin-walled steel tubes with much success. When high strength concrete and thin-walled steel tubes are used together, the more brittle nature of high strength concrete is partially mitigated by the confinement from the steel tube and local buckling of the thin steel tube is delayed by the support offered by the concrete which increase the strength, stiffness, and deformability of the section. Internal reinforcement is also used to enhance to the strength and facilitate connection to adjacent members [9].

A number of additional economic benefits stem from the use of CFTs:

- The tubes serve as formwork in construction which decreases labor and material cost
- In medium to high rising construction the building can ascend more quickly than a comparable reinforced concrete structure
- In high strength applications, smaller column sizes may be used increasing the amount of usable floor space in office buildings.

- The smaller and lighter framework places less of a load on the foundation, cutting cost again

These advantages have secured an expanding role for this versatile structural element in modern construction [5]. However, some factors complicate the analysis and design of concrete filled steel tube columns. A primary determent to wide spread use of CFTs is the limited knowledge regarding their behavior. A CFT member contains two materials with different stress- strain curves and distinctly different behavior. Interaction of the two materials possess a difficult problem in the determination of combined properties such as moment of inertia and modulus of elasticity. The failure mechanism largely depends on the shape, length, diameter, steel tube thickness, and concrete and steel strengths [8].

2.1 Analysis and Design of Composite Columns According to EBCS-EN1994-1-1:2013

EBCS EN 1994 gives two methods of composite columns design. These are "a general method" and "a simplified method". The general method can be applied for all types of composite columns including columns of non-symmetrical or non-uniform cross-sections over the column length. simplified method is applicable for columns of doubly symmetric and uniform cross section over the member length. Both methods of design assumed full interaction among the concrete, reinforcement steel and structural steel and hence plane sections remain plane while the column deforms up to failure.

The influence of local buckling of the steel section on the resistance shall be considered in design. The effects of local buckling for concrete filled steel cross-section provided for maximum values in the table are not exceeded.
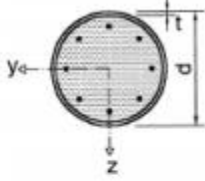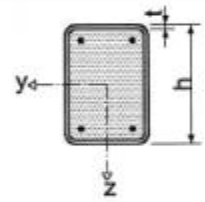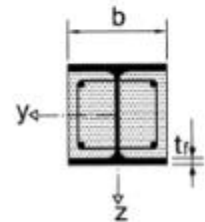
Cross-section		max (d/t), max (h/t) and max (b/t)
Circular hollow steel sections		max $(d/t) = 90\dfrac{235}{f_y}$
Rectangular hollow steel sections		max $(h/t) = 52\sqrt{\dfrac{235}{f_y}}$
Partially encased I-sections		max $(b/t_f) = 44\sqrt{\dfrac{235}{f_y}}$

Table 2-1 Maximum values of (d/t, h/t and /t$_f$) with f$_y$ in N/mm^2 [3]

2.1.1 Simplified Method of Design

To apply simplified method procedure of EBCS-EN 1994-1-1: 2013, the composite column has to fulfill the following criteria

- The member has to be doubly symmetrical and uniform cross section over the member length with rolled, cold-formed or welded steel sections.
- The simplified method is not applicable if the structural steel component consists of two or more unconnected sections
- The relative slenderness λ should be less than 2 ($\lambda \leq 2.0$)
- The longitudinal reinforcement that may be used in calculation should not exceed 6% of the concrete area.

- The ratio of the depth to the width of the composite cross-section should be within the limits 0.2 and 5.0. ($0.2 \le hc / bc \le 5.0$)

Resistance of cross sections and members in axial compression

- The plastic resistance of concrete filled sections to axial load $N_{pl,Rd}$ of a composite cross-section should be calculated by adding the plastic resistances of its components:

$$N_{pl,Rd} = A_a f_{yd} + 1.0 A_c f_{cd} + A_s f_{sd} \tag{2.1}$$

Where:

A_c is the cross-sectional area of concrete in the compression zone

A_s is the cross-sectional area of reinforcement bars

f_{cd} is design value of the cylinder compressive strength of concrete

f_{sd} is design value of the yield strength of reinforcing steel

For concrete filled tubes of circular cross-section,

- Increase in strength of concrete caused by confinement provided that the relative slenderness λ does not exceed 0.5 and e/d < 0, 1,

    Where: e is the eccentricity of loading given by MEd/Ned and

    d is the external diameter of the column.

- The plastic resistance to compression may then be calculated from the following expression:

$$N_{pl,Rd} = \eta_a A_a f_{yd} + A_c f_{cd} \left[1 + \eta_c \frac{t}{d} \frac{f_y}{f_{ck}} \right] + A_s f_{sd} \tag{2.2}$$

Where:

t is the wall thickness of the steel tube.

For members with e = 0 the values $\eta_a = \eta_{ao}$ and $\eta_c = \eta_{co}$ are given by the following expressions:

$$\eta_{ao} = 0.25\left(3 + 2\bar{\lambda}\right) \qquad \text{(but} \leq 1.0) \qquad (2.3)$$

$$\eta_{co} = 4.9 - 18.5\bar{\lambda} + 17\bar{\lambda}^2 \qquad \text{(but} \geq 0) \qquad (2.4)$$

For members in combined compression and bending with $0 < e/d \leq 0.1$, the values η_a and η_c should be determined from (2.5) and (2.6), where η_{ao} and η_{co} are given by (2.3) and (2.4):

$$\eta_a = \eta_{ao} + \left(1 - \eta_{ao}\right)(10e / d) \qquad (2.5)$$

$$\eta_c = \eta_{co}(1 - 10e / d) \qquad (2.6)$$

For e/d > 0.1, $\eta a = 1.0$ and $\eta c = 0$.

Due to member's imperfection, a column cannot carry an axial load as much as its section capacity. In addition to axial load, the column has to resist the associated imperfection moment. Thus, full section's axial load capacity of a column has to be reduced by a reduction factor. The reduction factors basically account for members' imperfection along with slenderness effect.

For simplification for members in axial compression, the design value of the normal force N_{ED} should satisfy:

$$\frac{N_{Ed}}{\chi Np_{l,Rd}} \leq 1.0 \qquad (2.7)$$

Where:

N_{ED} is the design value of the applied axial force

χ is the reduction factor for flexural buckling
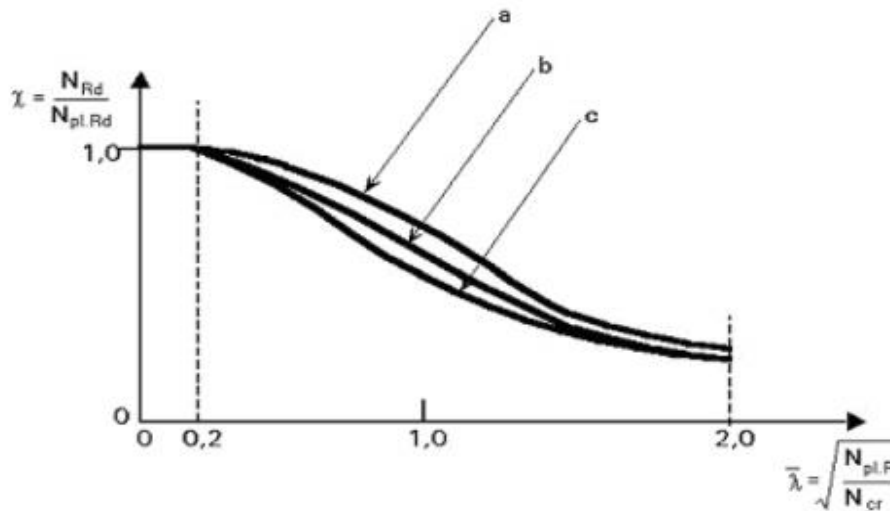
Figure 2.2 European buckling curve for composite columns [3]

$$\chi = \frac{1}{\phi + \sqrt{\phi^2 - \bar{\lambda}^2}} \le 1.0 \qquad\qquad (2.8)$$

$$\phi = 0.5\left[1 + \alpha\left(\bar{\lambda} - 0.2\right) + \bar{\lambda}^2\right] \qquad\qquad (2.9)$$

European bulking curve	a	b	c
Imperfection factor α	0.21	0.34	0.49

Table 2-2 Imperfection factor [3]

<u>Resistance of members in combined compression and uniaxial bending</u>

The capacity of a column cross section subjected to axial force and bending moment is determined from moment-axial force (M-N) interaction diagram. EBCS EN 1994, provides the plastic stress distribution of a fully encased cross-section for the points A to D as an example. In composite column interaction curve, the moment resistance increases up to the balanced point for a lower value of axial compression.

In the simplified method, the interaction curve is approximated by a polygonal made by connecting four or five points of the interaction curve.

Point A: represents the plastic axial load capacity of a composite section as given by equation

$$N_A = N_{pl,rd} \quad and \quad M_A = 0 \tag{2.10}$$

Point B: is the plastic moment resistance of a section.

$$N_B = 0 \quad and \quad M_B = M_{pl,rd} \tag{2.11}$$
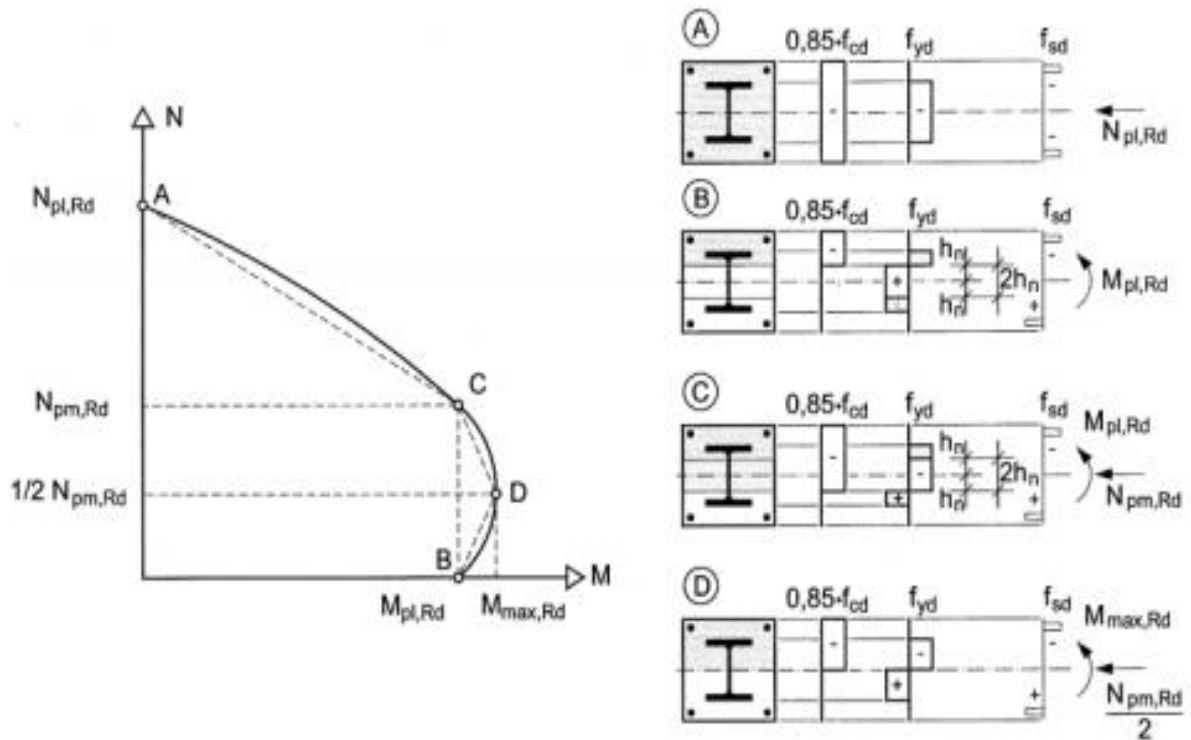
Figure 2.3 Simplified interaction curve and corresponding stress distributions for fully encased section [3]

Point C: corresponds to the same plastic moment resistance as point B but with resultant axial compression force. For concrete encased sections:

$$N_C = N_{pm,\,rd} = 0.85 * A_c * f_{cd} \quad and \quad M_C = M_{pm,\,rd} \tag{2.12}$$

Point D: is a balanced point representing the maximum moment carrying capacity of a composite section. For concrete encased sections:

$$N_D = 0.5 * N_{pm,rd} \quad and \quad M_D = M_{max,rd} \tag{2.13}$$

The resistance of a member to combined compression and bending is determined from its cross-section capacity curve including the influence of Imperfections.

The following expression based on the interaction curve determined according to should be satisfied:

$$\frac{M_{Ed}}{M_{Pl,N,Rd}} = \frac{M_{Ed}}{\mu_d M_{Pl,Rd}} \leq \alpha_M \tag{2.14}$$

Where:

M_{Ed} is the greatest of the end moments and the maximum bending moment within the column length, calculated including imperfections and second order effects if necessary

$M_{pl,N,Rd}$ is the plastic bending resistance taking into account the normal force N_{Ed}, given by

     $\mu_d M_{pl,Rd}.;$

$M_{pl,Rd}$ is the plastic bending resistance, given by point B in Figure 2

α_M is a correction factor for the non-conservative assumption that the rectangular stress block for concrete extends to the plastic neutral axis. For steel grades up to S355, α_M is 0.9 and for steel grades S420 and S460 α_M is 0.8.

The value $\mu_d > 1.0$ is recommended only if the bending moment M_{Ed} depends directly on the action of the design normal force $N_{Ed,}$ for example where the moment M_{Ed} results from an eccentricity of the normal force N_{Ed}. Otherwise an additional verification is necessary

in accordance with clause 6.7.1 (7) of EBCS-EN 1994-1-1: 2013, which states that, For composite compression members subjected to bending moments and normal forces resulting from independent actions, the partial factor γ_F for those internal forces that lead to an increase of resistance should be reduced by 20%.

2.2 Analytical and Experimental Investigations of Concrete Filled Steel Tubular Columns

2.2.1 Experimental investigations on axial load capacity of circular CFSTs

Experimental researches have been conducted worldwide for decades offering significant contribution to investigate the axial load capacity of CFST columns. Giakoumelis and Lam [10] tested 15 specimens to study axial capacity and the effect of bond strength between concrete and steel tube of short circular CFST columns with various concrete strengths under axial load. The degree of confinement offered by a thin-walled circular steel tube to the internal concrete was found to be dependent upon the loading condition. The results obtained indicated that when the steel and concrete were loaded together, the steel tube offered little confinement. Increased strength due to confinement of high-strength concrete was obtained only if the concrete is loaded and the steel is not bonded to the concrete. A series of tests had been carried out by Dundu [1] on the compressive strength of circular CFSTs with total of 24 specimens loaded concentrically in compression to failure. The results have shown that CFST columns having larger slenderness ratios failed by overall flexural buckling. Whereas the composite columns that have lower slenderness ratio failed by crushing of concrete and yielding of steel tube.

Schneider [11] investigated the effect of shapes of CFST column cross-sections (3 circulars, 5 square and 6 rectangular) and wall thickness of the steel tube on the compressive resistance of concentrically loaded short composite columns. Both steel tube and concrete core were loaded simultaneously. The results obtained showed that composite columns constructed from circular hollow sections offered better post yield concrete

confinement, stiffness and ductility compared to the rectangular and square hollow sections. Specimen with larger wall thickness had higher stiffness than those with smaller thickness. Similar results were also obtained by O'Shea and Bridge [12] and Giakoumelis and Lam [10]. Ekmekyapar and AL-Eliwi [13] come up with a different conclusion after conducting experiment on CFSTs that, D/t and confinement factor do not have direct impact on CFST column behavior.

2.2.2 Finite Element analysis of circular CFSTs

In order to simulate the behavior of concrete-filled steel tube columns a nonlinear finite element model using the ABAQUS program is common in most of the reviewed researches. Schneider [11] developed a Three-dimensional nonlinear finite element models to further study the axial load behavior of CFTs. The concrete core of the CFT was modeled using 20-node brick elements, while The steel tube was modeled using an 8-node shell element. Moon et al. [9] used 4-node shell element (S4R) to model the steel shell. Some other researchers might disagree with modeling steel tube of CFSTs using shell elements. To provide proper curved contact boundary between concrete core and steel tube single layer of C3D8R element is preferable instead of shell elements [14]. Other analytical study suggests to model compact steel tubes, solid elements were found to be more efficient in modeling both the steel tube and the concrete as well as the clearly defined boundaries of their elements [15]. Ellobody et al. [15] used three-dimensional eight-node solid elements (C3D8) to model both steel tube and concrete core. Yonas et al. [16] also modeled both material with 8-node solid elements (C3D8). For top and bottom rigid plates a 4-node discrete rigid element (R3D4) was used [14]. The purpose of placing the rigid plates on the top and bottom of the CFST column section is to simulate the real conditions of composite column while distributing the applied axial load uniformly throw-out the cross-section of both steel tube and concrete [16]. Rigid part represents that a part is so much stiffer than the rest that deformation can be considered negligible [17]. Ellobody et al. [15] tried different mesh sizes in order to find a reasonable mesh that provides both accurate results and less computational time. It is found that a mesh size of 1:1:2 for length, width and depth respectively, for most of the elements, can achieve accurate results. On the other side

even though finer mesh provides very accurate results but mesh size of 20 mm can give acceptable results [14]. Yonas et al. [16] also used mesh size of 20mm which is chosen based on a convergence analysis and recommends assigning similar mesh size for all elements in order to get accurate results.

Concrete core due to confining steel tube is to undergo a state of Tri-axial stresses and hence exhibit higher compressive strength. This can be mainly attributed to the degree of confinement to the strain hardening behavior of the steel material. So to simulate the tri-axial state of concrete core uniaxial stress-strain curve is used and the concrete core response under axial loading is simulated using the damaged plasticity model available in ABAQUS material library. A multi linear stress-strain curve is employed to simulate the response of steel material [18].

Concrete is represented by a transversely isotropic body that is under conditions of tri-axial compression by axial stresses and transversal stresses. The form of the diagram is assumed to be curvilinear with a descending branch [18].

The dilation angle, ψ, of the concrete is an important model parameter, which in part determines the plastic hardening of the concrete. It was approximated as 20° [9]. Abbas [19] proposed empirical formula to calculate the value of dilation angle. The default dilation angle in ABAQUS which is 36° was used to represent the inclination that the plastic potential reaches for high confining pressure for concrete filled steel tube [16]. The uniaxial behavior of the steel tube can be simulated by an elastic-perfectly plastic model with an associated flow rule. When the steel tube is subjected to multiple stresses, a von Mises yield criterion, is employed to define the elastic limit [20]. For simplicity, stress-strain curve of steel is idealized as trilinear curve. The curve is divided into three parts with three linear curves. First part of the curve is elastic in nature up to the yield point with slope equal to the elastic modulus of steel and The second part is constant at yield stress fy which is plastic in nature. The third part of the curve shows the strain hardening εt in steel ending up to ultimate stress   and ultimate strain εu of steel [14].

Schneider [11] used the interface, or gap, element available in ABAQUS, for the interface between the concrete and the steel components. The GAP element has infinite stiffness for the compression and no stiffness in tension, which permitted simulation of slip by separation of two nodes. (Penetration of one node into an adjacent one was prevented.) The normal stresses in the GAP element results in confinement of the concrete, thus it permits explicit modeling of the confining effect of the tube [9]. The interface element allows the surfaces to separate under the influence of a tensile force. However, the two contact elements are not allowed to penetrate each other [15]. Yonas et al. [16] defines tie constraints for the interface between steel and concrete. The interaction is assumed to be fully bonded and hence tie constraints were adopted. For interaction, surface to surface contact was created between steel tube and concrete core with tangential behavior. Penalty method (also known as stiffness method) was used for imposing frictional constraints. This stiffness method allows the relative motion between the surfaces of two materials even when they are sticking [14].

The differences between the simulated and measured test results are likely due to several factors. First, it is almost impossible to achieve ideal pin-ended support in experiments due to the friction generated between the test specimen and the test setup. Second, the exact shape and magnitude of initial imperfection are unknown and cannot be applied to the finite-element models. These factors indicate the finite-element models used in this study provide a suitable, conservative estimate of the buckling strength of CFTs [9].

2.2.3 Strength of circular CFT columns under axial compression

The CFT column power resistance is the work of the concrete and steel shell under the conditions of a volumetric stress state. As the loading level increases, the stress state changes not only quantitatively but also qualitatively. Therefore, the dependencies between the stresses and strains for concrete and steel are not known before the calculation begins. In this regard, the deformation calculation of the CFTC strength is proposed to be conducted in two stages [18]. The failure modes of all CFST hybrid columns can be characterized as compression failure, whole of the specimen shows the axial compression

deformation, obvious local buckling was observed at the end of each column [21]. Unusually, the distortional buckling can occur for longitudinally stiffened circular sections in which the bond strength between the concrete and longitudinal stiffeners in a compression zone is not sufficient to resist the resulting force occurring at the stiffeners from the outward expansion of the concrete under compression and/or bending. In practice, distortional buckling is rarely found in circular CFT columns [22]. EC4 [4] states that the effects of local buckling should be considered in design for slender sections exceeding the maximum D/t limit.
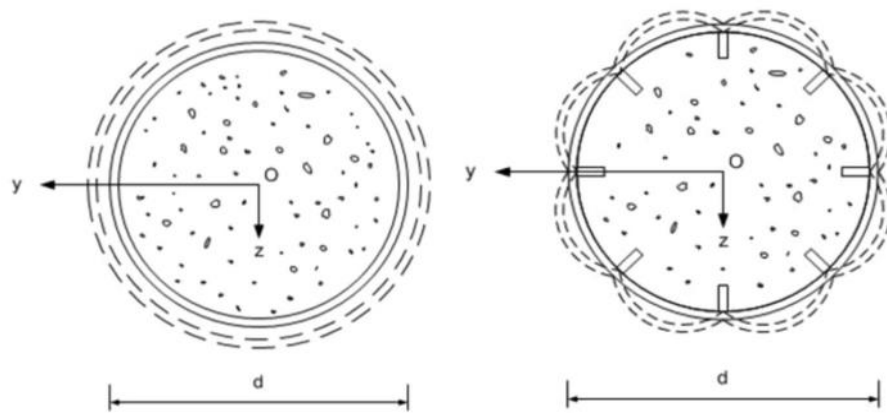
Figure 2.4 Local buckling modes of circular CFT columns [22].

Another parametric study reveals that critical buckling loads of CFST columns are very much affected by the diameter-to-depth ratio and concrete elastic modulus. Moreover, material nonlinearity has a pronounced effect for short CFST columns, and a negligible effect for slender ones [23].

The maximum value of a compression force is taken as a bearing capacity that is reached in the process of an incrementing relative deformation of shortening in the most compressed fiber with a normal section [18]. local buckling shape, stress distribution, and cracking pattern shows that the steel tube fully yielded in tension and compression region and the maximum compression was observed at the tip of the compression part [9].

2.2.4 Interaction curve for CFST columns

To assess the strength of CFTs under axial loading, either the plastic-stress distribution or strain compatibility methods are used in different codes. Eurocode 4 [4] reported that the plastic-stress distribution method is the method of choice for its simplicity and accuracy. Only EC4 uses concrete design strength that is increased by multiplying the concrete nominal compressive strength with the amplification factor to account for hoop tension in circular CFT columns. The plastic-stress distribution method is an equilibrium based method used to determine the strength of a CFT member where instability effects due to global buckling are not considered [9]. Axial compression-uniaxial bending interaction curve for CFT column cross section can be found by considering different positions of the neutral axis over the whole cross section and by determining the internal action effects from the resulting stress distributions. Kwon and Park [22] developed the simplified strength interaction curves for a circular CFT column, which are quite similar to those for compact sections in the EC4.
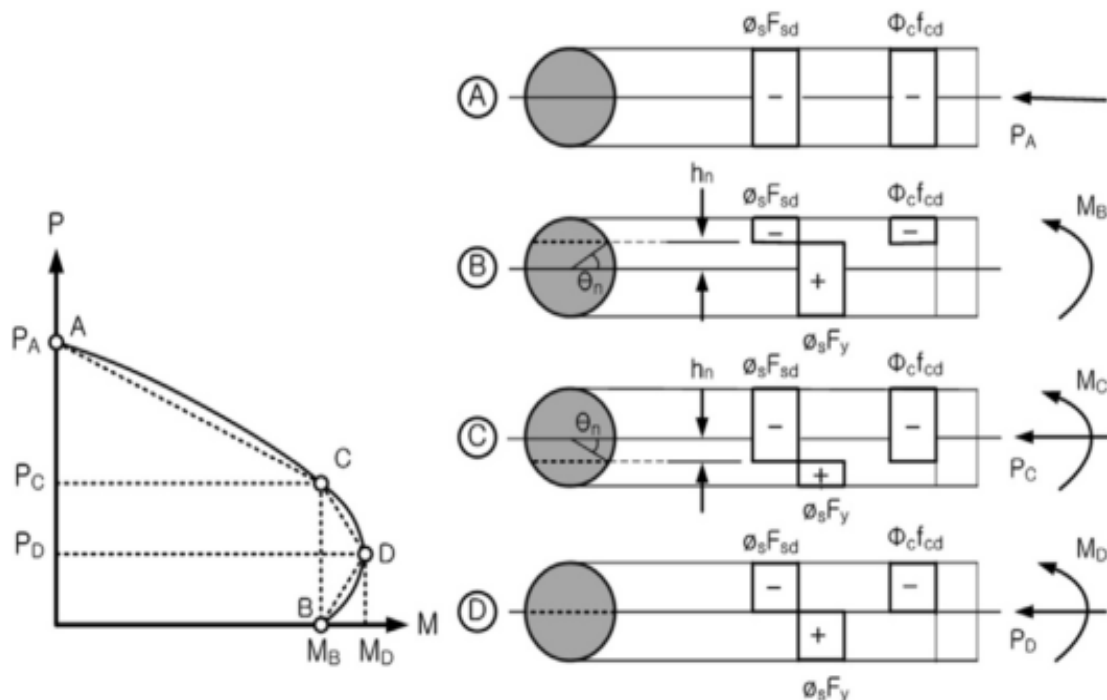
Figure 2.5 P-M Strength interaction curve for circular CFST [22].

The effect of steel reinforcement was neglected for all cases that considered and therefore the constructed interaction curves are on the safe side [24].

In many related researches P-M interaction curves for CFSTs are developed based on finite element analysis results. Axial load capacity of CFST column modeled in ABAQUS are obtained from the analysis outputs. From analysis and the experiments, moment capacity of CFST columns is not directly obtained. The moments from the analysis are computed by multiplying the axial forces with the total eccentricities at the mid-height (initial eccentricity of the undeformed specimens plus the additional eccentricity due to lateral bending of the specimens) [25]. The global analysis on a 3D-model is a geometric and material nonlinear analysis with imperfections and must include 2nd order effects and imperfections (geometric and residual stresses) [26]. The P-Delta effect or the 2nd order effect or the non-linear geometry in the analysis is considered by using the updated Lagrangian formulation [25]. The results from both the experiments and numerical investigation were compared with the axial load versus moment capacity curve (P-M capacity curve) generated using a fiber-based model as suggested in Eurocode 4. plastic-stress distribution method provides accurate and conservative predictions of the strength of the CFT when the axial load is low, but it had been noted, this method significantly overestimates the strength with high axial load and slenderness ratio, because global buckling is not considered in the P-M interaction curves from the plastic-stress distribution method. When the axial load exceeds buckling capacity, the plastic stress distribution method overestimates the moment capacity of the CFT. In this study, P-Δ effects were included in the moment calculations for all comparisons [9]. P- M curves obtained by 3DNLFEA and concrete damaged plasticity model in ABAQUS are showing good prediction on the P-M capacity curve at the peak stress. However, as the load increases, the P-M capacity curves from the analysis and experiments are outside the P-M capacity curve of Eurocode 4 [25]. P-M capacity curve using Eurocode 4 is found to be conservative. While conservatism is desirable, it has negative consequences with seismic design. Seismic design requires consideration of the expected capacity of ductile elements. most practical columns have relatively small axial load ratios and the Eurocode 4 interaction curves

considerably underestimate the moment capacity of CFTs under these conditions. This results in increased uncertainty as to the expected moment capacity of the member and requires greater conservatism in the seismic design. Taken as a whole, these results suggest a need to improve the P-M interaction curve to provide a more economical and rational design [9].

CHAPTER THREE

RESEARCH METHODOLOGY

3.1 Research Design

The research methodology in this paper consists of numerical modeling of circular CFST columns. Outputs from the finite element analysis are used to compute axial load and moment capacity of each CFST column section and further employed in constructing interaction charts. The cross-sections used in this thesis are checked to fulfill the simplified method of analysis given in the code EBCS EN 1994-1-1:2013. Diameters and thickness of steel tube were selected from the circular hollow section (CHS) properties provided in the structural steel sections table. The diameter to wall thickness ratio was checked to be less than the maximum D/t value for circular hollow steel section specified in EBCS EN 1994-1-1:2013.

$$\max\left(d/t\right) = 90\,\frac{235}{f_y} \tag{3.1}$$

for $f_y = 355$MPa, *Max (D/t) = 59.58*

All the CFST columns analyzed in this study have the same structural steel grade of S 355 H and concrete grade of C-30. Both the top and bottom rigid plates have a thickness of 50mm.

3.2 Study Variables

3.2.1 Independent variables

The independent variables or parameters that were studied include:

- CFSTs without reinforcing steel bars
- Diameters circular CFST cross-section
- Length of column
- Varies thicknesses of steel tube

- Steel reinforcement ratio

3.2.2 Dependent Variables

- Axial load and moment capacity of CFST columns
- Interaction diagrams for circular CFST columns

3.3 Data Source and Presentation

The parameters were inspected by finite element analysis. outputs obtained from the ABAQUS analysis were further used to develop interaction diagram which gives the combination of axial load and moment required to cause failure of a column. So results are presented by interaction charts which represent resistance of the column section for combined axial load and bending for various steel ratio and diameters of CSFT columns.

3.4 Finite Element Modeling

The finite element analysis program ABAQUS, 2017 is used for the numerical simulation of circular concrete filled steel tubular columns. In order to simulate the actual behavior and represent the real loading condition, the steel tube, concrete core and the interaction constraints have to be modeled properly. The choice of suitable element type and mesh size that can possibly provide acceptable results with reasonable computational time is also important in numerical analysis.

3.4.1 Finite Element Type and Mesh

After reviewing prior literatures, solid elements were found to be more efficient to model both steel tube and concrete core. Also the CFST was provided with two rigid plates at top and bottom with their respective reference points (nodes). From sets of standard elements provided in ABAQUS, the eight-node solid element (C3D8R) was used to model both steel tube and concrete. A discrete rigid element of 4-node 3D bilinear rigid quadrilateral (R3D4) was used to model the top and bottom plates.
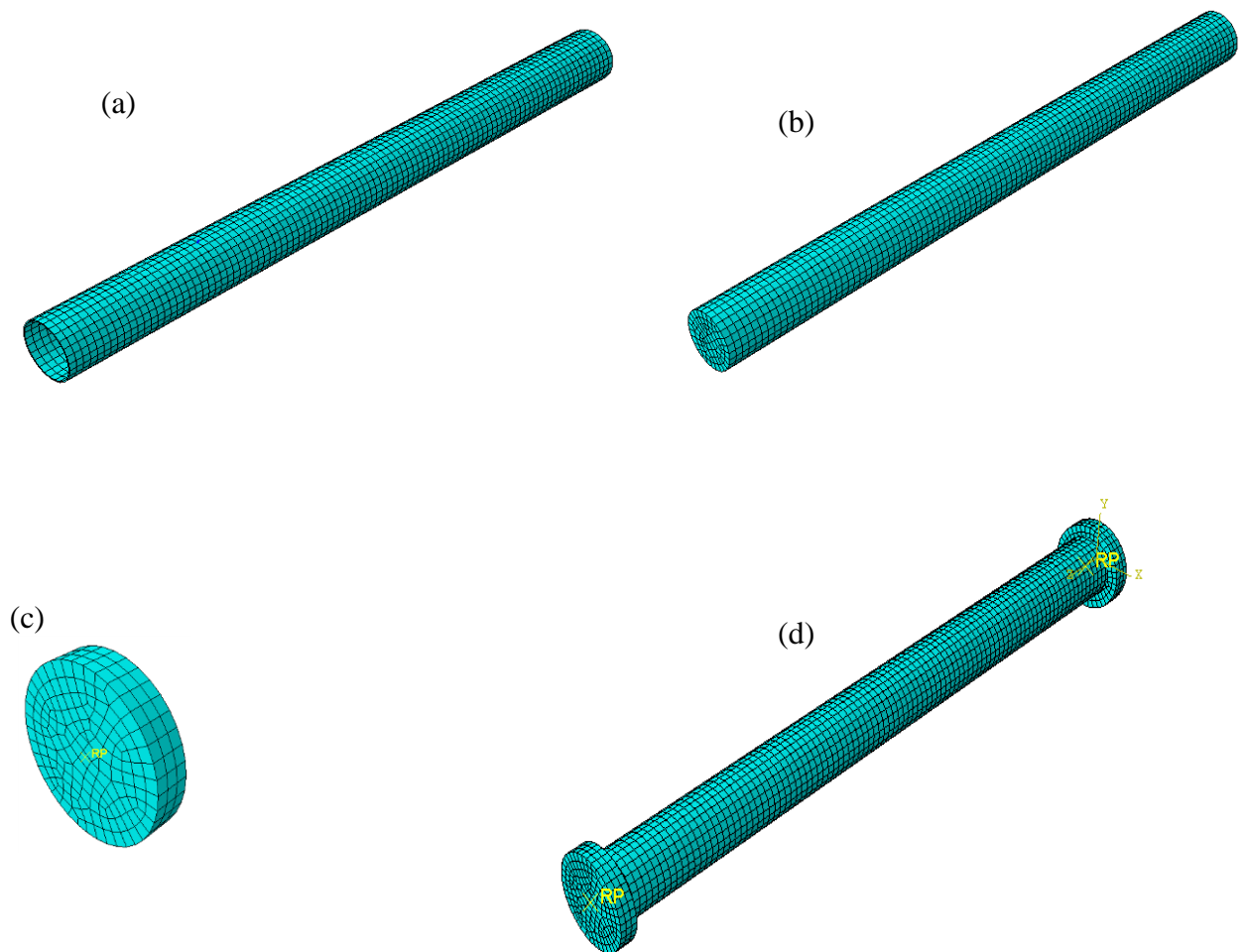
Figure 3.1 Finite element mesh of analytical model circular concrete-filled steel tube column: (a) Steel Tube, 8-node solid element; (b) Concrete infill, 8-node solid element; (c) Loading plate (Base plate): 4-node discrete rigid element; (d) Assembled CFST model

The mesh size is kept 20mm for all four parts. Obviously, finer mesh gives quite accurate results but the analysis could take extended computational time. The mesh size of 20mm provides relatively accurate and acceptable results along with reasonable analysis running time.

3.4.2 Materials

3.4.2.1 Steel Tube

Tri-linear stress-strain curve is idealized to simulate the response of steel tube with isotropic hardening plasticity rule. The first section of the curve represents elastic behavior of steel until the proportional limit stress reaches the yield point with slope of Young's Modulus taken to be 205 GPa and Poisson's ratio approximated to be 0.3.
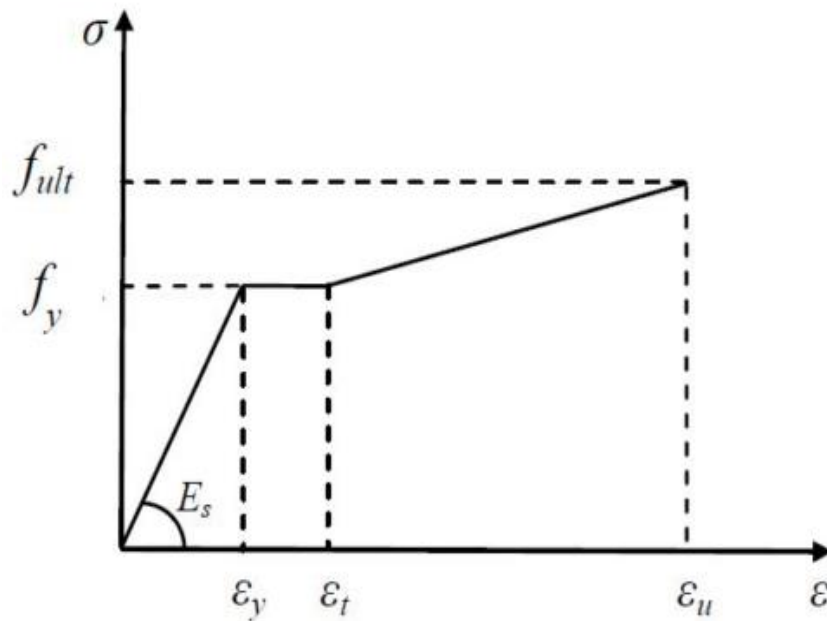
Figure 3.2 Trilinear stress-strain curve for steel [14].

The second part of the curve have constant yield stress, fy which represents plastic nature. The third part shows strain hardening in steel which remains up to the ultimate stress, f_{ult} and ultimate strain, ε_u. The ultimate strain, ε_u of the steel tube is assumed to be equal to 0.2.

3.4.2.2 Concrete

Due to confining effect of the steel tube, the concrete core undergoes tri-axial stresses. In order to simulate the tri-axial state of concrete, uniaxial stress-strain curve is considered. The first part is the initially assumed elastic range to the proportional limit stress. The mean compressive strength, fcm is used to plot the curve. Secant modulus of confined concrete, Ecm is calculated using the empirical Equation given by EBCS EN 1992-1-1:2013.
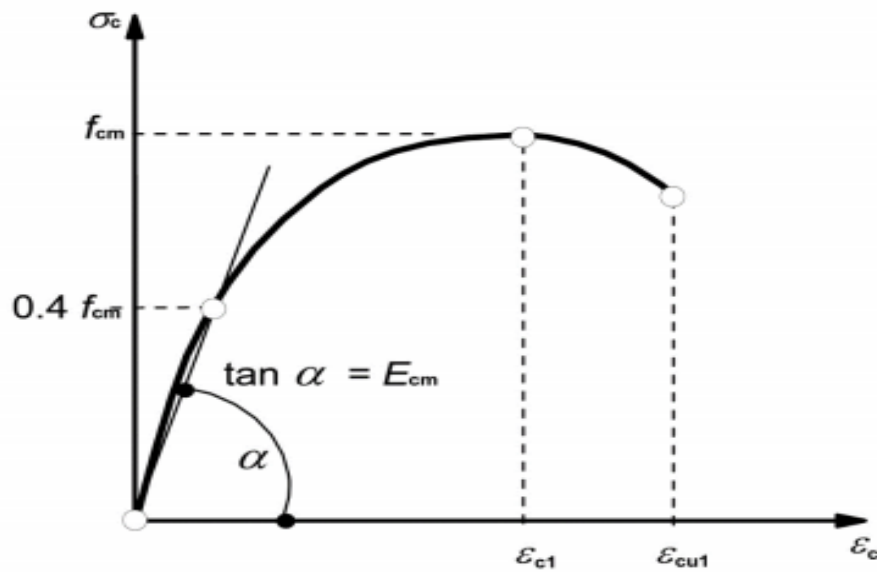
Figure 3.3 Schematic representative of the stress-strain relation of structural analysis [27]

$$f_{Cm} = f_{Ck} + 8 \qquad\qquad (3.2)$$

$$E_{Cm} = 22 \left(\frac{f_{Cm}}{10} \right)^{0.3} \qquad\qquad (3.3)$$

A constitutive model based on the combination of damaged mechanics and plasticity is developed to analyze the failure of concrete. Yielding part of the confined stress-strain curve represent behavior of concrete after proportional limit stress. To account for the non-linear and plastic behavior of concrete, the modified Druncker-Prager yield criterion which is concrete damaged plasticity model available in ABAQUS material library was defined.

Damaged plasticity model consists of dilation angle (ψ) which determines the plastic hardening of concrete, ratio of concrete compressive strength under bi-axial and uniaxial loading conditions (f_{bo}/f_{co}), and the ratio of the second invariant on the tensile meridian to that on the compressive meridian (K). Based on prior researches the values of those parameters in this study are taken as follows:

Dilation angle, ψ	Eccentricity	f_{bo}/f_{co}	K	viscosity
36º	0.1	1.16	0.667	0

Table 3-1 Input material data for concrete damaged plasticity

The relation of compressive stress, δ_c and shortening strain, ε_c for short term uniaxial loading is described by the expression

$$\frac{\sigma_c}{f_{cm}} = \frac{k\eta_-\eta^2}{1 + (k-2)\eta}$$

(3.4)

- $k = 1.05 E_{cm} \frac{\varepsilon_{c_1}}{f_{cm}}$ (3.4a)

- $\eta = \frac{\varepsilon_c}{\varepsilon_{c_1}}$ (3.4b)

- $\varepsilon_{c_1} = 0.7(f_{cm})^{0.31}$ (3.4c)

Where:

f_{cm} mean compressive strength

k factor

E_{cm} secant modulus of elasticity

ε_{c1} peak strain

ε_c ultimate strain
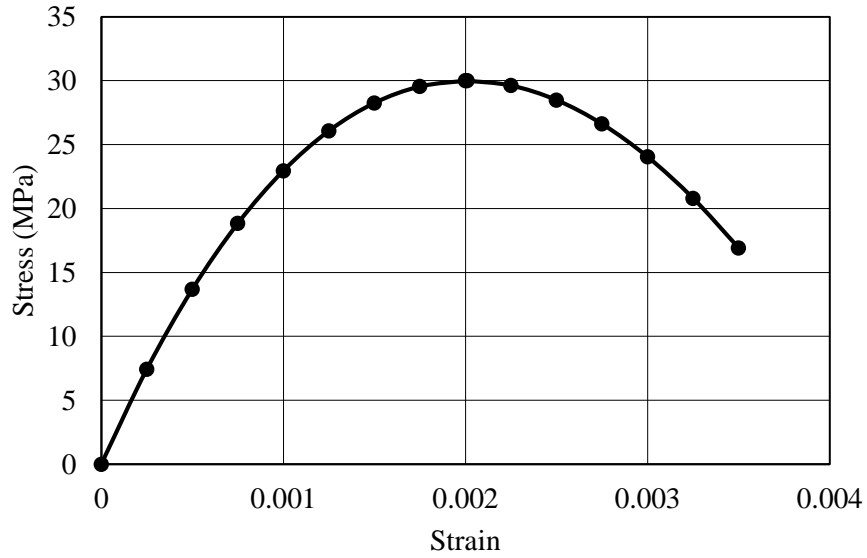
Figure 3.4 Stress-Strain curve for compressive behavior of the analyzed concrete

The tensile behavior of concrete is defined in terms of fracture energy and crack opening displacement.

$$\frac{\sigma}{f_t} = f(w) - \frac{w}{w_c} f(w_c)$$

(3.5)

$$f_t = 0.3 f_{cm}^{\frac{2}{3}}$$
(3.5a)

$$f(w) = \left[1 + \left(\frac{C_1 w}{w_c}\right)^3\right] \exp\left(\frac{C_2 w}{w_c}\right)$$
(3.5b)

$$w_c = \frac{5.14 G_f}{f_t}$$
(3.5c)

$$G_f = 73. f_{cm}^{0.18}$$
(3.5d)

Where:

f_t Tensile strength

w Crack displacement

w_c Critical crack opening displacement

G_f Fracture energy (energy required to develop unit area of crack)

c_1 & c_2 Factors
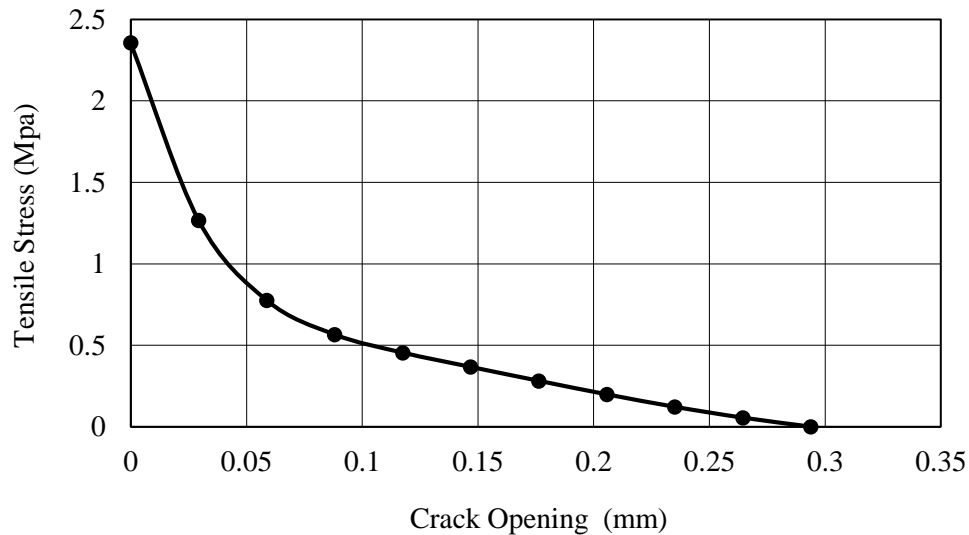
Figure 3.5 Tensile stress-crack opening curve for the tensile behavior of concrete

The compressive and tensile stresses with their respective inelastic strains and crack displacements are calculated using the above equations. compression and tension damage values were also computed. Those are input values used to define behavior of concrete in the damaged plasticity model.

3.4.3 Step and Interaction Properties

Beside to the initial step in which boundary conditions are defined, additional step, Step-1 is created to apply the axial loading. Static, general procedure is selected and the total time period has set to be 1. Nlgeom, setting is turned on to account for geometric nonlinearity. 'Maximum number of increments' and 'minimum increment size' could have different values depending on the required incrimination to complete a specific analysis. While the initial increment size is set to be 0.01.

Tie constraints were created for the interaction between the steel tube and concrete infill. Hence full bonding without slip or sliding condition is idealized at the interface of the two parts. So both steel and concrete sections are acting as a single unit. Tie constraints were

also assigned between each rigid plates with top and bottom nodes of both steel and concrete.

3.4.4 Boundary Condition and Load Application

The boundary conditions at the top and bottom plates of the circular CFST columns were kept fixed against all degrees of freedom except for the displacement at the loading plate in the direction of axial deformation.

The load was exerted at reference node of the top loading plate by applying point displacement of 100mm. For columns modeled without rigid plates, static uniform load was applied using displacement control at each node of the loaded top surface. To achieve eccentrically loading condition, the rigid plates were assembled such that their centroids coincide 'e' distance away from centroid of the cross-section. The load incrimination and iterative equation solving is based on the Newton-Raphson method.

Table 3-2 Dimensions of circular CFST columns selected for analysis

Model	D (mm)	t (mm)	L (mm)	D/t	L/D
M-1	168.3	3.2	2000	52.59	11.88
M-2	168.3	3.2	2500	52.59	14.85
M-3	168.3	3.2	3000	52.59	17.83
M-4	168.3	3.2	3500	52.59	20.80
M-5	168.3	3.2	4000	52.59	23.77
M-6	168.3	5	2000	33.66	11.88
M-7	168.3	5	3500	33.66	20.80
M-8	168.3	6.3	3000	26.71	17.83
M-9	168.3	6.3	4000	26.71	23.77
M-10	193.7	5	2000	38.74	10.33
M-11	193.7	5	3000	38.74	15.49
M-12	244.5	5	2000	48.90	8.18
M-13	244.5	5	3000	48.90	12.27
M-14	244.5	8	3500	30.56	14.31
M-15	244.5	8	4000	30.56	16.36

A total of 15 circular CFST column models under concentric axial compression were analyzed. In addition, eccentrically loading conditions were simulated for eccentricity, e= (20mm, 30mm, 40mm & 50mm)

3.5 Interaction Chart Development procedures for Axial Compression and Uniaxial Bending

From the result outputs of the CFST column numerical analysis, nodal reaction forces and mid-height displacements have been utilized as main inputs to construct N-M interaction charts. Unlike axial load capacity, moment capacity is not directly obtained from the FE analysis. In this study moment capacity of CFST column section was computed by multiplying axial force obtained from FE outputs with the total eccentricities (initial eccentricity of the un-deformed specimens plus the additional eccentricity due to lateral bending of the analytical models of circular CFST columns).

$$M = P(e + \Delta) \qquad\qquad (3.6)$$

Most of the analytic columns in this thesis are loaded concentrically but when column drifts the applied axial load will likely become eccentric since the nodes of the member have moved 'Δ' distance sideways. This causes additional stress to the members which induces bending moment over the column section. So in this study, P-Δ effects were mainly included for moment calculations.

EC-4 based N-M interaction diagram has been computed for comparison. This interaction chart is drawn using the stress blocks that show the plastic section capacity of composite cross-sections. The fundamental equations used here are from the design aid for circular concrete filled steel composite columns proposed by Ketema [28].

CHAPTER FOUR

RESULTS AND DISCUSSIONS

This section presents results from the numerical analysis and verifications of the finite element model in comparison with previously conducted experimental researches and Eurocode 4. The outputs monitored includes:

- Deformed shapes of the CFST column models together with Von-Mises yield criterion of steel tube, hardening parameters and confining pressure of the concrete core.
- Reaction force (axial load capacity) of each column section
- Mid-height displacement (lateral deflection) of the circular CFST column

4.1 Model Verification

In order to check the validity of finite element analysis, behavior of circular CFST columns analyzed in prior experimental test results were used to verify the FE analytical models under axial compression. The validations are carried out by comparing the failure modes and load-displacement curves obtained from FE analysis outputs with experimental results. The verification was extended to include comparisons between the compressive resistance resulted from test and numerical analysis with EC-4 proposed calculation of axial load capacity for circular CFST columns. The experimental load–axial displacement curves were compared with the numerical results, and good agreement had been achieved.

Three tested specimens were used for verification. The first two specimens (C-1 & C-7) were tested by Giakouleris and Lam [10]. For the third specimen (S1-5) selected, the experiment was conducted by Dundu [1] to assess compressive strength of circular CFST column. Summarized result of verification is presented as follows.

Specimen	Dimensions					Material Properties				Researcher
	D (mm)	t (mm)	L (mm)	D/t	L/D	Concrete strength (Mpa)	Steel tube fy (Mpa)	Ec (Gpa)	Es (Gpa)	
C-1	114	3.87	300	29.4	2.62	_	343	_	205	Giakoumelis and Lam
C-7	115	5	300	23	2.61	30	365	30.6	205	
S1-5	127.3	3	1000	42.43	7.86	30	345	31.1	209	M. Dundu

Table 4-1 Dimensions and material properties of Verified specimens

1) Specimen C-1 (steel tube without concrete infill)
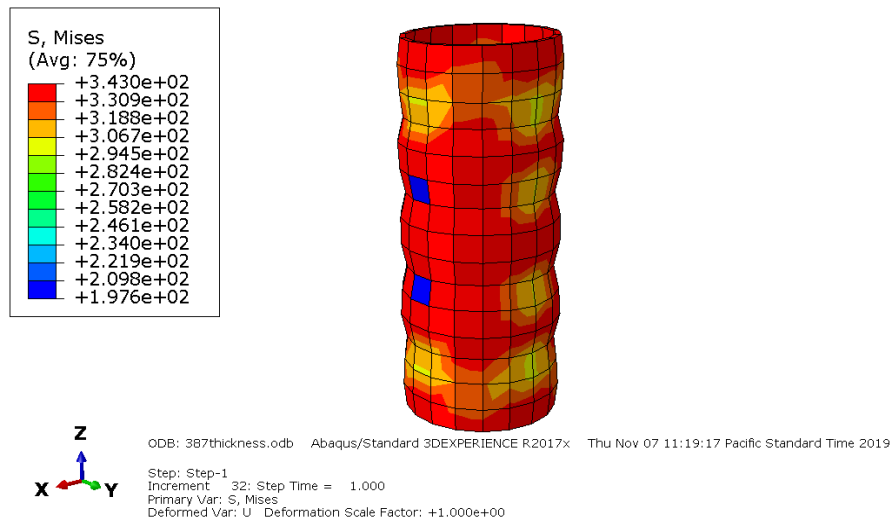
Figure 4.1 Failure mode of C-1 column modeled in ABAQUS

Axial load capacity of specimen C-1 from the experimental result was 539 KN [10] while the finite element analysis gives 522 KN. Figure 4.2 plots the load–axial shortening curves for C-1.
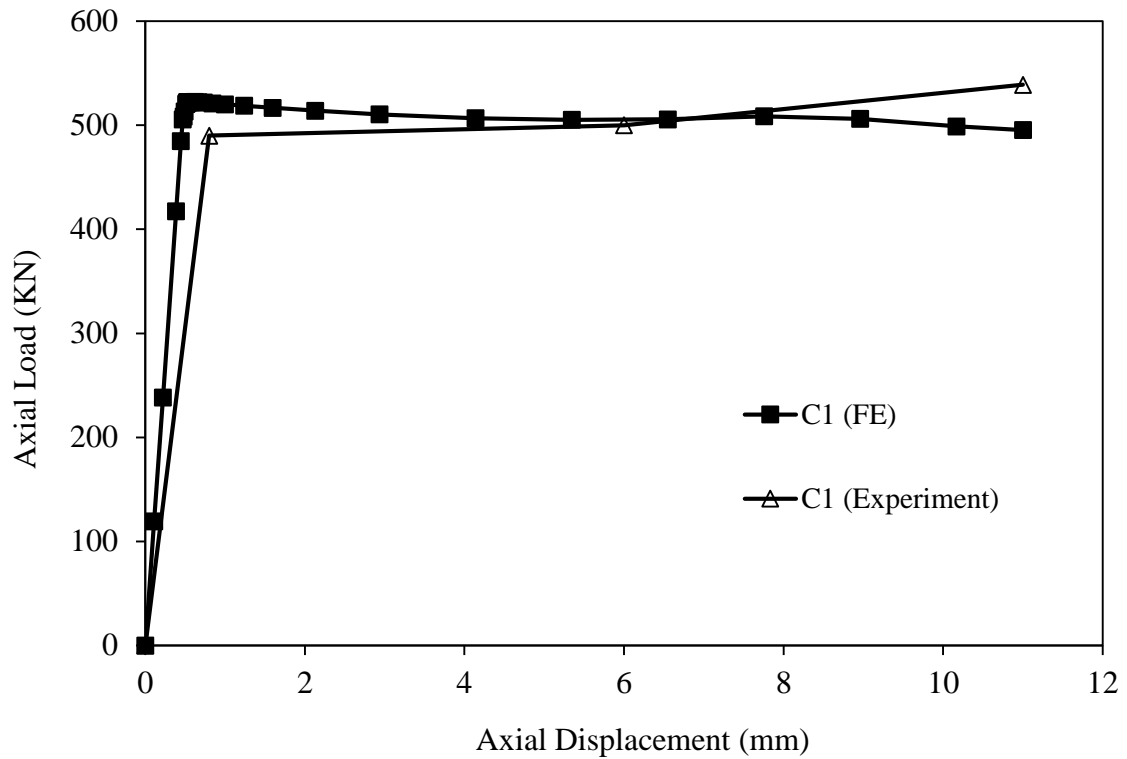
Figure 4.3 Load-displacement curve for FEA and experimental analysis of C-1

2)   Specimen C-7
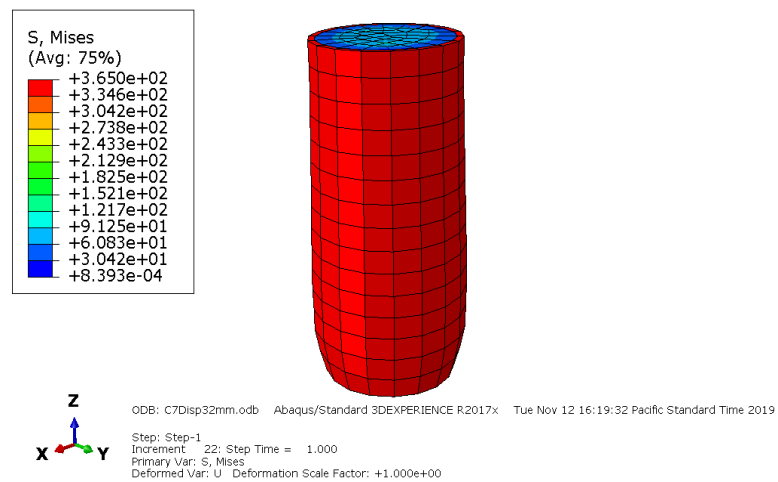
Figure 4.4 Failure mode of C-7 column modeled in ABAQUS

Axial load capacity of specimen C-7 from the experimental result was 1380 KN [10] while the finite element analysis gives 1362 KN. Figure 4.4 plots the load–axial shortening curves for C-7. It can be seen that the finite element model successfully predicted the ultimate load of the columns and the load–axial shortening behavior.
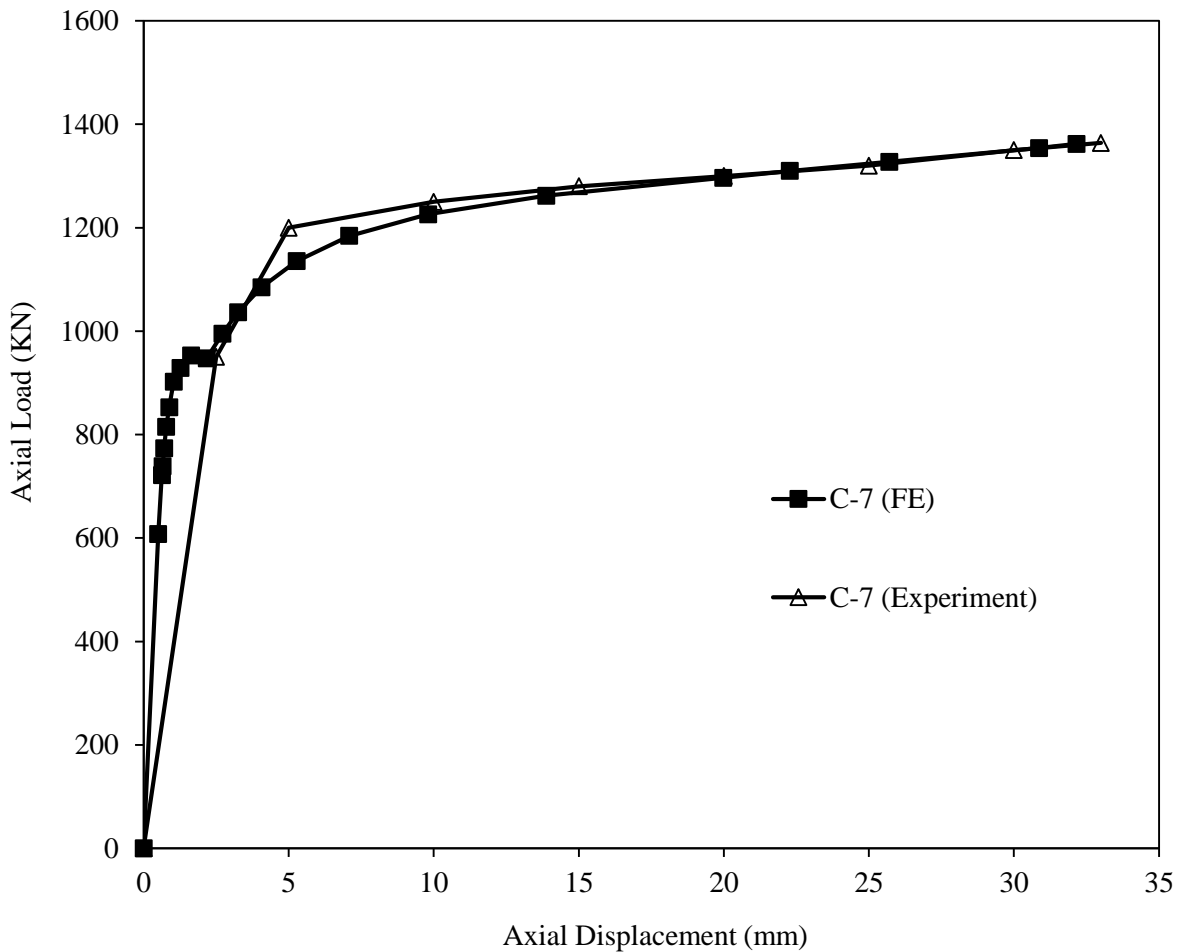
Figure 4.5 Load-Displacement curve comparison between FEA and experimental analysis for C-7

3) Specimen S1-5

Axial load capacity of specimen S1-5from the experimental result was 912.1 KN [1] and result of the ABAQUS analysis gives 1000 KN. Figure 4.5 plots the load–axial displacement curves illustrating comparison of experimental and finite element analysis for S1-5.
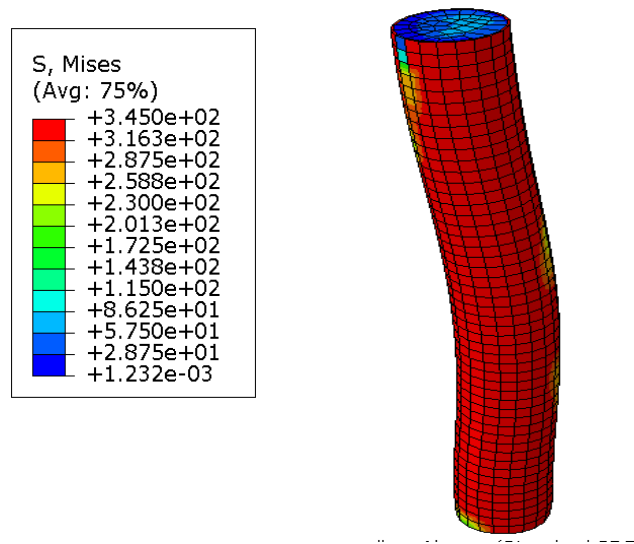
Figure 4.6 Comparison of deformed shape from experimental and finite element analysis, S1-5
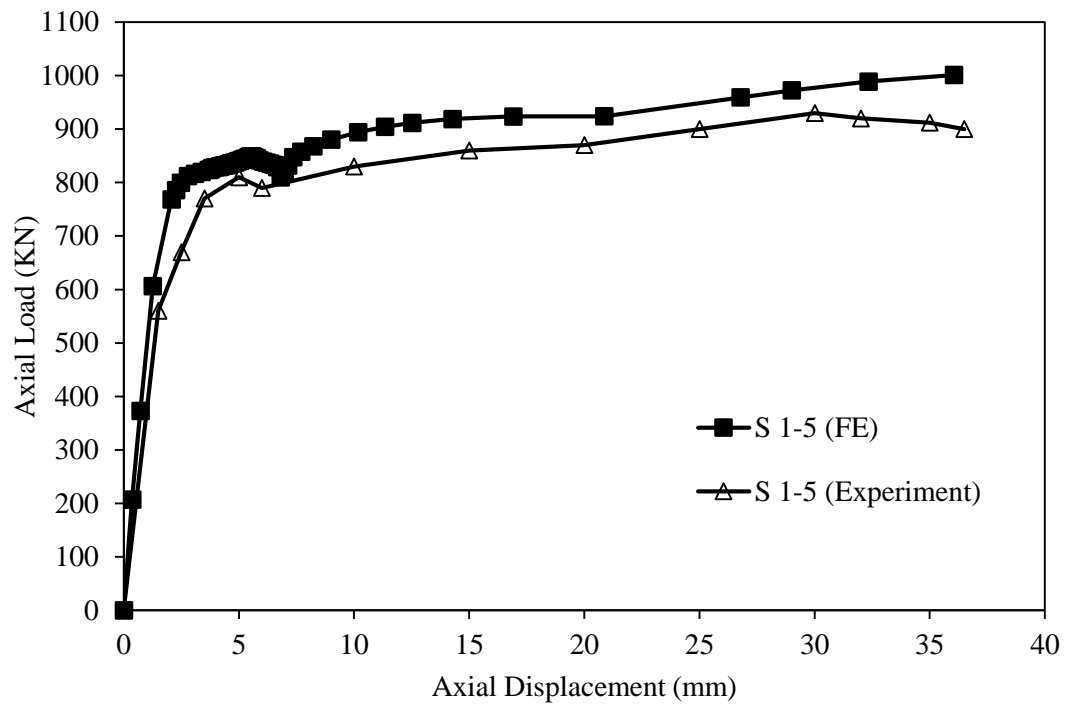
Figure 4.7 Load-Displacement curve comparison between FEA and experimental analysis for S1-5.

The observed locations and shapes of the local buckling and load-displacement curves are found to be almost similar to the simulated responses. The comparisons are summarized in the table below.

Specimen	N_{Test} (KN)	N_{FE} (KN)	N_{EC4} (KN)	$\dfrac{N_{Test}}{N_{FE}}$	$\dfrac{N_{Test}}{N_{EC4}}$	$\dfrac{N_{FE}}{N_{EC4}}$
C-1	539	522	474.13	1.03	1.13	1.1
C-7	1380	1362	1134.2	1.01	1.21	1.2
S1-5	912.1	1000	775	0.91	1.17	1.3

Table 4-2 Comparisons of results from experimental analysis with Finite Element and EC-4 results for CCFST columns under axial load

4.2 Finite Element Analysis Outputs

The result presented in figure 4.8 is taken from the FE analysis of M-1 which was modeled with diameter D=168.3mm, thickness of steel tube t=3.2mm and length of column L=2000mm
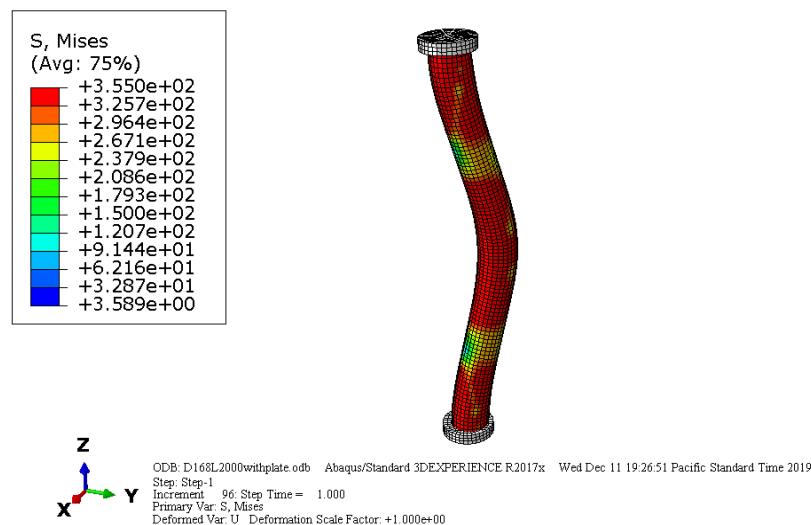
Figure 4.8 Von-Mises stress distribution for M-1

As it is observed from the figure, the Von-Mises stress has reached yield stress of steel tube. Another analytic representation of the lateral displacement (deflection) of M-1 is also presented. It is shown that the maximum deflection is at mid-height section of the CCFST column.

D/t=52.6

D=168.3mm & t=3.2mm

Axial load capacity, *RF= 1415KN*
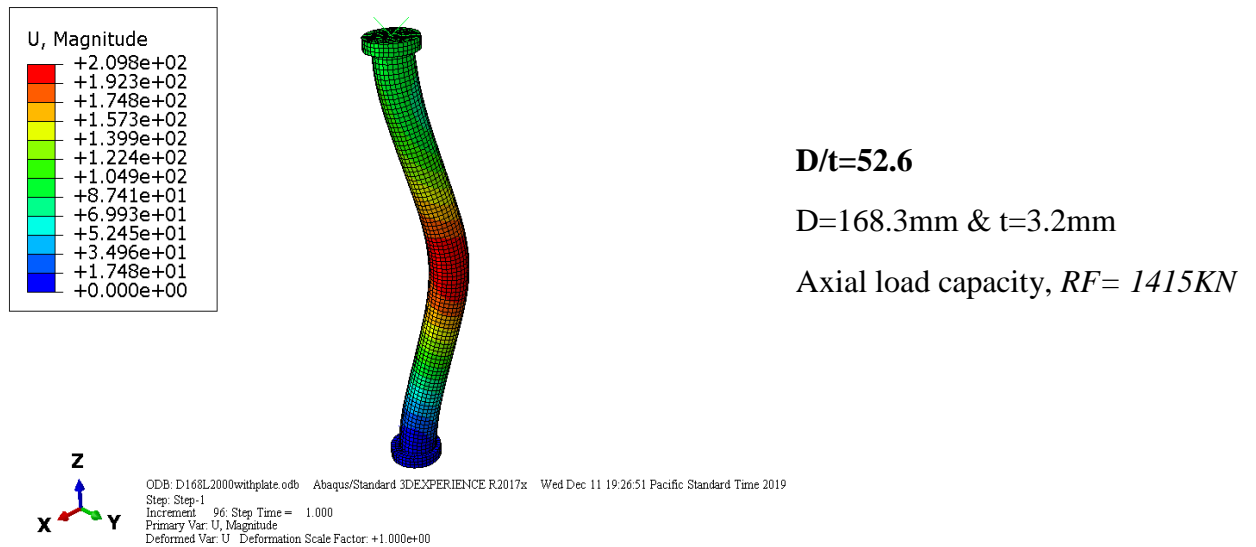
Figure 4.9 Mid-height deflection for M-1

4.2.1 Effect of column length in CCFST analysis

Length of column has a significant effect on the strength and deformation behavour of CCFST. In the figure below, M-5 is modeled having the same loading condition and cross-sectional dimensions with the privious one but length of column L=4000mm. It is shown that Mid-height displacement increases as a result of the increased length.

U, Magnitude
+3.806e+02
+3.489e+02
+3.171e+02
+2.854e+02
+2.537e+02
+2.220e+02
+1.903e+02
+1.586e+02
+1.269e+02
+9.514e+01
+6.343e+01
+3.171e+01
+0.000e+00

ODB: D168L4000.odb   Abaqus/Standard 3DEXPERIENCE R2017x   Tue Dec 03 20:27:14 Pacific Standard Time 2019
Step: Step-1
Increment   425: Step Time =   1.000
Primary Var: U, Magnitude
Deformed Var: U   Deformation Scale Factor: +1.000e+00

Figure 4.10 Mid-height deflection for M-5

4.2.2 Effect of steel-tube thickness in CCFST analysis

Thickness of steel-tube highly contributes for the load carrying capacity of CCFST column. Steel-tube Thicknesses used for this study are varied from t=3.2mm to t=8mm. The variation is assigned with respect to column diameter. From the numerical analysis, it is observed that axial load capacity of the circular concrete filled steel column increases as thickness of steel-tube increases. For example, while keeping other parameters all the same (D=168.3mm & L=2000mm), except for steel-tube thickness increases from 3.2mm to 5mm; the axial load capacity of the column (M-6) increased by 33.2%.it is also observed that, magnitude of mid-height deflection decreases for the CCFST with 5mm steel-tube thickness, which is illustrated in the figure below.

D/t=33.66

D=168.3mm & t=5mm

Axial load capacity, *RF= 1768KN*
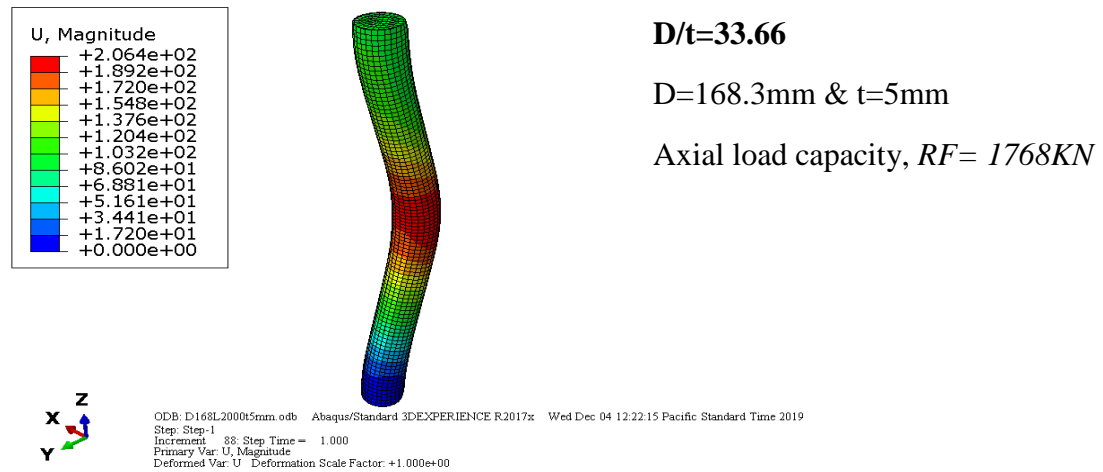
Figure 4.11 Mid-height deflection for M-6

4.2.3 Effect of eccentric loading on CCFST column strength and magnitude of lateral displacement

The load Eccentricities studied in this thesis include, **e**= (20mm, 30mm,40mm & 50mm). The effect of eccentricl loading were assessed for the CCFST model having D=168.3mm, t=3.2mm & L=2000mm. while eccentricity increases, axial load capacity of CCFST column decreases by 4% as compared with the concentric loading (e=0) condition of the same model.
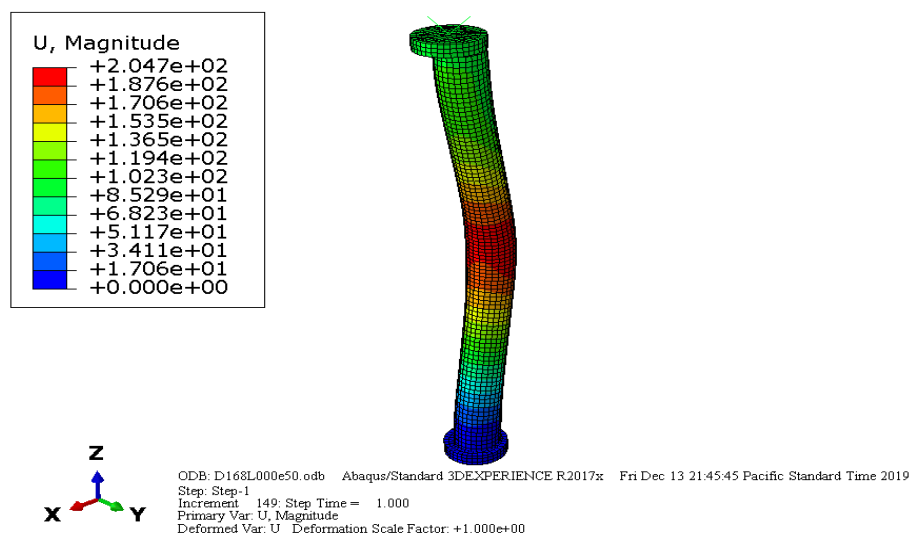
Figure 4.12 Mid-height deflection for M-1 under load eccentricity, e=20mm
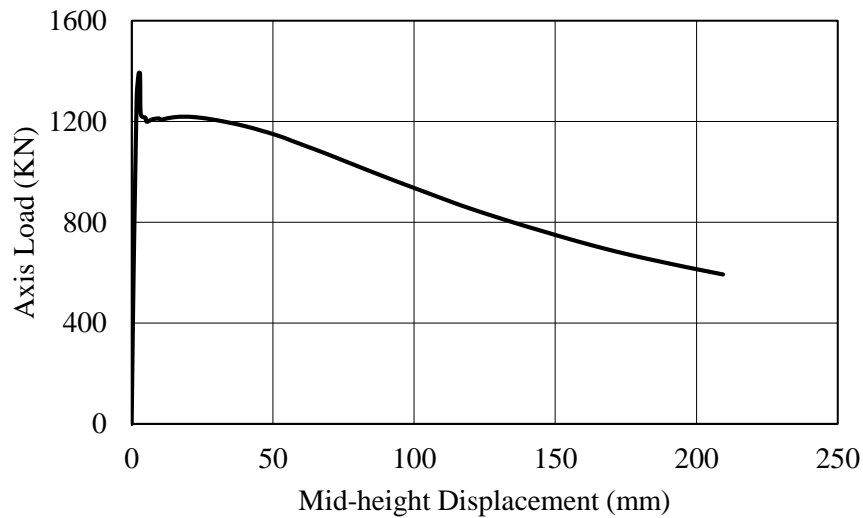
Figure 4.13 Load vs Mid-height displacement curve for loading eccentricity, e=20mm

4.2.4 Effect of diameter to thickness (D/t) ratio on axial load capacity and magnitude of lateral displacement

In this thesis CCFSTs having three different diameters were analyzed (168.3mm, 193.7mm & 244.5mm). The respective D/t ratios studied varied from 26.71mm to 52.59mm. It is obvious that circular CFST columns with maximum Diameter and thickness, have high load carrying capacity and minimized magnitude of deflection; since increased cross-sectional area stiffens column under axial compression. Stress distribution, load capacity and magnitude of mid-height displacement results from the FEA are presented to illustrate contribution of diameter and tube thickness for the strength of CCFST columns.

D/t=48.9

D=244.5mm & t=5mm

Axial load capacity, *RF= 3420KN*
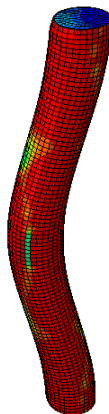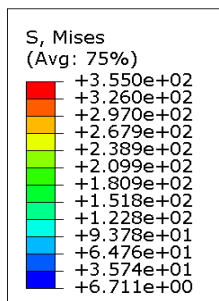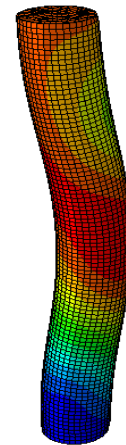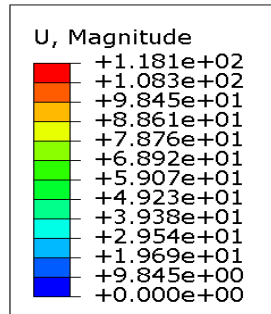
D/t=38.74

D=193.7mm & t=5mm

Axial load capacity, *RF= 2400KN*

Figure 4.14 Results from simulated CCFST analytic models with t=5mm and
D=244.5mm & 193.7mm respectively

4.3 N-M Interaction Diagram Development

In this section axial load vs bending moment interaction charts for circular concrete filled steel tubular columns with varies D/t and steel ratios are presented. The charts are generated in MS-Excel.

Interaction curve construction using simplified method of EC-4 based calculation have been conducted for comparison. The CCFST model M-1 is selected for the EC-4 method of developing N-M interaction diagram.

Table 4-3 Material property data for steel and concrete

Material Properties Of Steel Tube (N/mm^2)		Material Properties Of Concrete (N/mm^2)	
F_u	510	f_{cu}	30
F_{yk}	355	f_{ck}	24
F_{yd}	322.727	f_{cd}	16

Steel Ratio; $w = \dfrac{A_s f_{yd}}{A_c f_{Cd}}$

Table 4-4 Cross-sectional dimensions and computed steel ratio of analyzed CCFSTs

D (mm)	D_i (mm)	As (mm^2)	Ac (mm^2)	t (mm)	w
168.3	161.9	1659.77	20586.6	3.2	1.6
168.3	158.3	2565.12	19681.25	5	2.6
168.3	155.7	3206.32	19040.05	6.3	3.5
193.7	183.7	2964.03	26503.86	5	2.3
244.5	234.5	3761.96	43189.34	5	2
244.5	228.5	5943.79	41007.5	8	3

For EC-4 based simplified method of uniaxial interaction chart construction, the analytic model with; D=168.3mm t=3.2mm is selected. P-M capacity curve is generated using a fiber-based model as suggested in Eurocode 4. As stated in the methodology section, The fundamental equations used are from the design aid for circular concrete filled steel composite columns proposed by Ermiyas Ketema [28].

For Circular Concrete Filled Steel Tube Column:
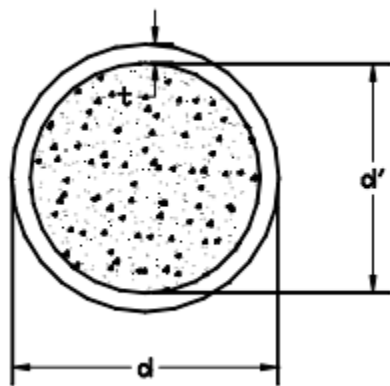
Figure 4.15 circular concrete filled steel cross-section

$$w = \frac{A_s f_{yd}}{A_c f_{cd}}$$

$$A_s f_{y_d} = w A_c f_{cd}$$

$$A_c = \frac{\pi d'^2}{4} \quad where \ d' = d - 2t$$

$$A_s = \frac{\pi d^2}{4} - A_c$$

Moment and axial load capacity for different neutral axis positions

Moment and axial load capacity can be computed from assumed neutral axis positions. Each position of the neutral axis represents one point in the interaction curve for section capacity. Sufficient points are developed to get a smooth curve that represents the capacity of a given cross-section. Three different cases of neutral axis position are selected.

Case I: The whole cross section under compression.

a) Axial load capacity

$$N_U = N_{p_{l,rd}}$$

$$N_{p_{l,rd}} = A_c f_{cd} + A_s f_{yd}$$

$$A_c = \frac{\pi d'^2}{4} \qquad \& \qquad A_s = \frac{\pi d^2}{4} - A_c$$

$$A_c = \frac{\pi(161.9)^2}{4} \qquad \Rightarrow Ac = 20586.6 \ mm^2$$

$$A_s = \frac{\pi(168.3)^2}{4} - 20586.6 \ mm2 \qquad \Rightarrow As = 1659.77 \ mm^2$$

$$\Rightarrow N_{pl, \, Rd} = 865 \ KN$$

$$\Rightarrow v = \frac{N_{p_{l,rd}}}{A_c f_{cd}} \qquad v{=}2.63$$

b) Moment capacity

Since the whole part is in compression the moment capacity is zero.

➤ $M_{pl, Rd} = 0$, $\mu = 0$

Case II: More than half the cross-section under compression
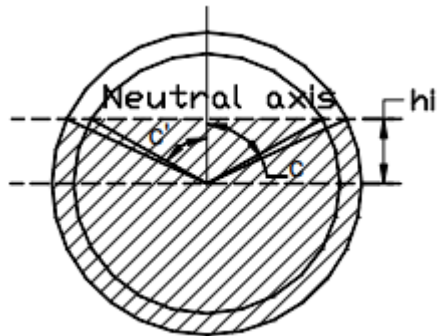
Figure 4.16 Neutral axis position for $0 \le hi \le d/2\text{-}t$

Area and Section Modulus for a Segment
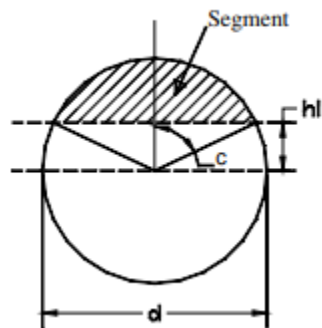
Figure 4.17 Segment of a Circle

$$c = \cos^{-1}(\frac{2h_i}{d})$$

Area of segment; $A_{seg} = C(d/2)^2 - h_i \tan c$

Section modulus of segment; $W_{Seg} = \frac{2}{3}(\frac{d^3}{8}\sin c - h_i^3 \tan c)$

Thus, applying these equations for concrete filled tubes

Section modulus of concrete part of the segment; $W_{Segc} = \frac{2}{3}(\frac{d'^3}{8} \sin c - h_i^3 \tan c')$

Where $c' = \cos^{-1}(\frac{2h_i}{d'})$

Section modulus of steel part of the segment; $W_{Sega} = \frac{2}{3}(\frac{d^3}{8} \sin c - h_i^3 \tan c) - W_{Segc}$

a) Axial load capacity

$N_u = A_{CC} f_{cd} + A_{Snet} f_{yd}$

$A_{CC} = \pi \left(d'/2\right)^2 - \left\{C' \left(d'/2\right)^2 - h_i^2 \tan C'\right\}$

$A_{Snet} = 0.25\pi(d^2 - d'^2) - 2[\{c\left(d/2\right)^2 - h_i^2 \tan c\} - \{C' \left(d'/2\right)^2 - h_i^2 \tan C'\}]$

$\Rightarrow v = \frac{N_U}{A_C f_{cd}}$

b) Moment capacity

$M_u = 2 \times W_{Sega} f_{yd} + W_{Segc} f_{cd}$

$\Rightarrow \mu = \frac{M_u}{A_C f_{Cd} \frac{d'}{2}}$

Table 4-5 Nu and Mu computation for case-II

h_i	$W_{seg, a}$	$W_{seg,c}$	A_{cc}	A_{snet}	N_u (KN)	M_u (KNm)	ν	μ
0	43618.3	353638.3	10293.27	0	164.6924	33.8	0.50	1.3
5	40845.0	354309.7	11102.26	64.04	198.3046	32.0	0.60	1.2
10	32586.4	356284.9	11908.15	128.32	231.9424	26.7	0.70	1.0
15	19027.8	359446.2	12707.8	193.08	265.636	18.0	0.81	0.68
20	484.0	363592.5	13498.02	258.58	299.4184	6.1	0.91	0.23
25	-22590.6	368431.6	14275.48	325.11	333.3298	-8.7	1.01	-0.33
30	-49586.7	373568.2	15036.68	393.01	367.4206	-26.0	1.12	-0.98
35	-79716.9	378485.6	15777.91	462.65	401.7566	-45.4	1.22	-1.7
40	-111981.2	382517.1	16495.13	534.52	436.4263	-66.2	1.32	-2.5
45	-145114.0	384802.9	17183.88	609.21	471.5519	-87.5	1.43	-3.3
50	-177500.5	384219.7	17839.12	687.52	507.308	-108.4	1.54	-4.1
55	-207037.3	379260.3	18455	770.54	543.9535	-127.6	1.65	-4.8
60	-230877.5	367809.9	19024.43	859.87	581.8936	-143.1	1.77	-5.4
65	-244912.7	346677.3	19538.38	958.07	621.8101	-152.5	1.89	-5.7
70	-242504.8	310418.7	19984.45	1069.75	664.9881	-151.6	2.02	-5.7
75	-210258.0	247304.7	20343.05	1205.03	714.3828	-131.8	2.17	-4.9
80	-94925.0	106778.3	20570.87	1400.84	781.2211	-59.6	2.37	-2.2
80.95	8095.7	0	20586.55	1462.87	801.4929	5.2	2.43	0.2

Case III: *Less than half the area under compression*
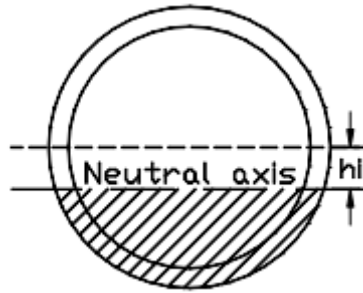
Figure 4.18 Neutral axis position with $0 \leq hi \leq d/2\text{-}t$

a) Axial load capacity

$$N_u = A_{CC}f_{cd} + A_{Snet}f_{yd}$$

$$A_{CC} = \left\{ C' \left(\frac{d'}{2} \right)^2 - h_i^2 \tan C' \right\}$$

$$A_{Snet} = 0.25\pi(d^2 - d'^2) - 2[\left\{ c\left(\frac{d}{2} \right)^2 - h_i^2 \tan c \right\} - \left\{ C' \left(\frac{d'}{2} \right)^2 - h_i^2 \tan C' \right\}$$

$$\Rightarrow v = \frac{N_U}{A_cf_{cd}}$$

b) Moment capacity

The moment capacity is the same as that is given in case II

Table 4-6 Nu and Mu computation for case-III

h_i	A_{cc}	A_{snet}	N_u (KN)	v
0	10293.28	0	164.7	0.50
5	9484.29	64.04	172.4	0.52
10	8678.40	128.32	180.3	0.55
15	7878.75	193.08	188.4	0.57
20	7088.53	258.58	196.9	0.60
25	6311.07	325.11	205.9	0.63
30	5549.87	393.01	215.6	0.65
35	4808.64	462.65	226.2	0.69
40	4091.42	534.52	238.0	0.72
45	3402.67	609.21	251.1	0.76
50	2747.43	687.52	265.8	0.81
55	2131.5	770.54	282.8	0.86
60	1562.12	859.87	302.5	0.92
65	1048.17	958.07	326.0	0.99
70	602.1	1069.75	354.9	1.08
75	243.5	1205.02	392.8	1.19
80	15.68	1400.83	452.3	1.37
80.95	0	1462.87	472.1	1.43
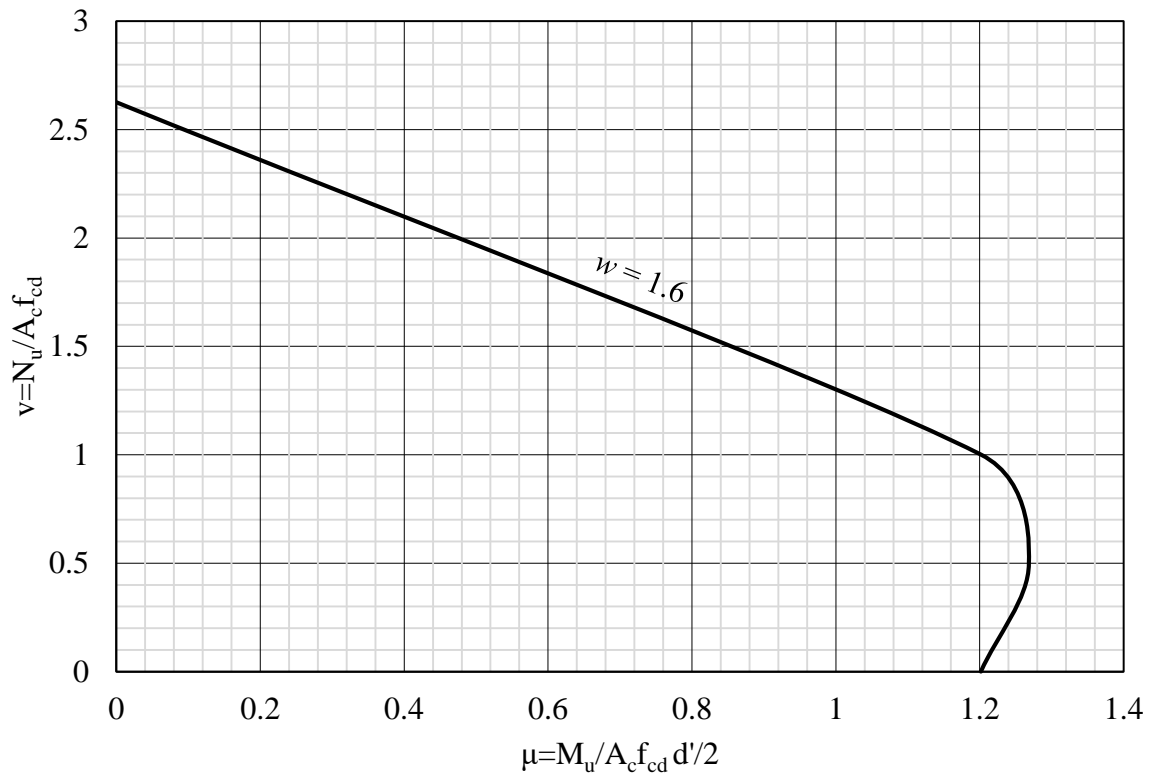
Figure 4.19 Uniaxial chart for circular CFST column section using Eurocode 4 method of N-M calculation (D/t=52.6, w=1.6)

As noted previously Eurocode 4 suggests a method for tracing interaction diagram based on the plastic stress distribution method. Uniaxial charts representing strength of circular concrete filled steel composite column computed using EC-4 method is presented in the figure. Axial load and moment interaction diagram developed from numerical (ABAQUS) analysis has been compared with EC-4 predicted resistance. From the comparisons, N-M capacity curve using EC-4 tends to be more conservative. While the conservatism of the code strength prediction might be desirable to avoid premature failure in seismic design. However, EC-4 interaction curve considerably underestimates the moment and load capacity of CFSTs under axial load which will not provide economical and rational design.

In the comparison uniaxial chart presented below, strength interaction curve from the finite element analysis is outside the N-M capacity curve of Eurocode 4.
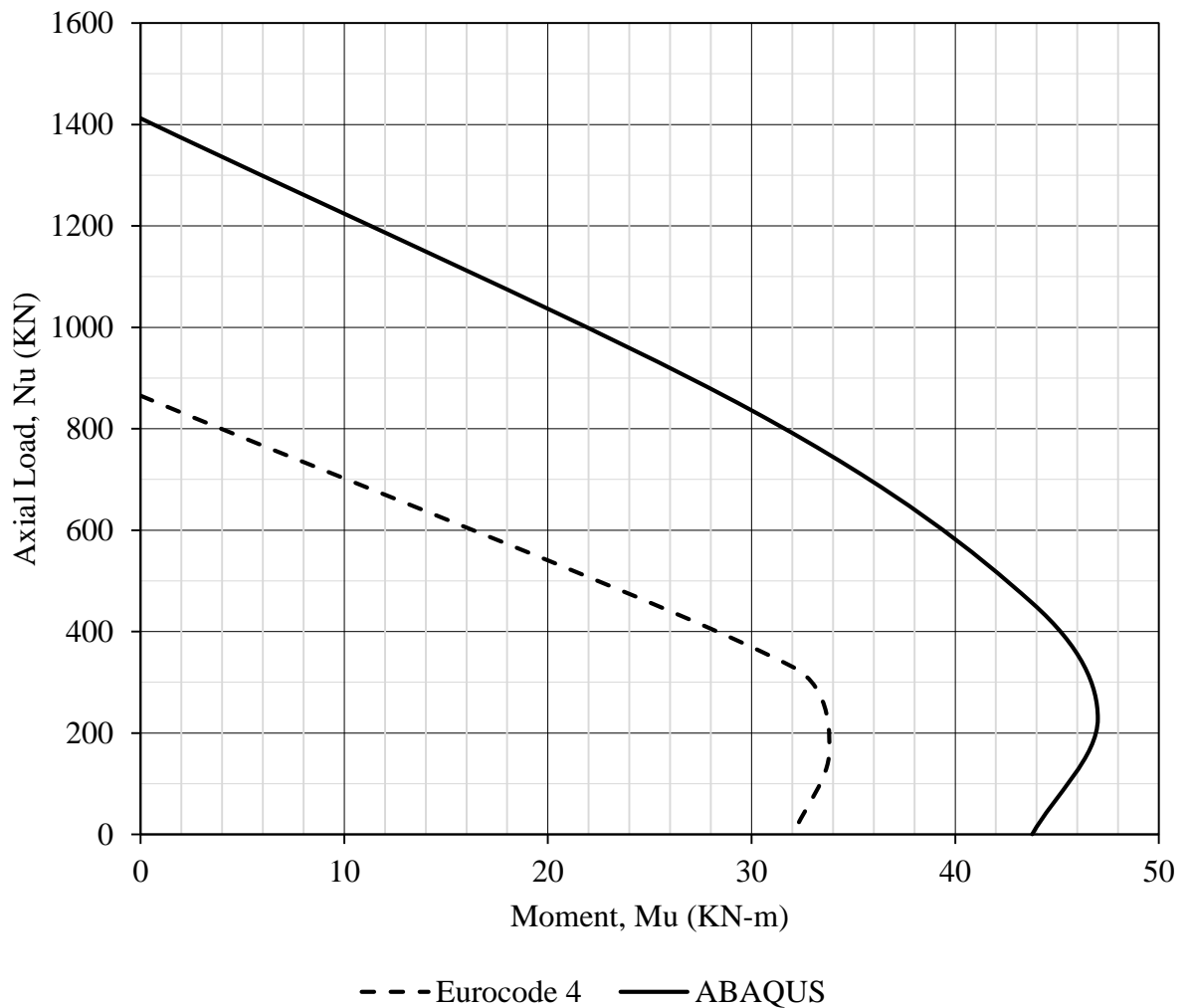
Figure 4.20 Comparison of N-M interaction curves constructed from EC-4 & ABAQUS analysis results (D/t= 52.6, w=1.6)

The possible reason for numerical analysis giving maximum column strength values as compared with EC-4 results is;

- ➢ In ABAQUS analysis, plastic behavior of both materials including the damaged plasticity model for concrete have been defined. The assigned behavior extends to consider tensile strength of concrete and strain hardening conditions by establishing compressive and tensile damaged parameters. These material properties used in FE analysis promote increased section stiffness and higher load resistance capacity for the modeled circular concrete infilled steel tubular column.

4.3.1 Uniaxial interaction chart of normalized axial load and moment capacity for varying steel ratio, *w*
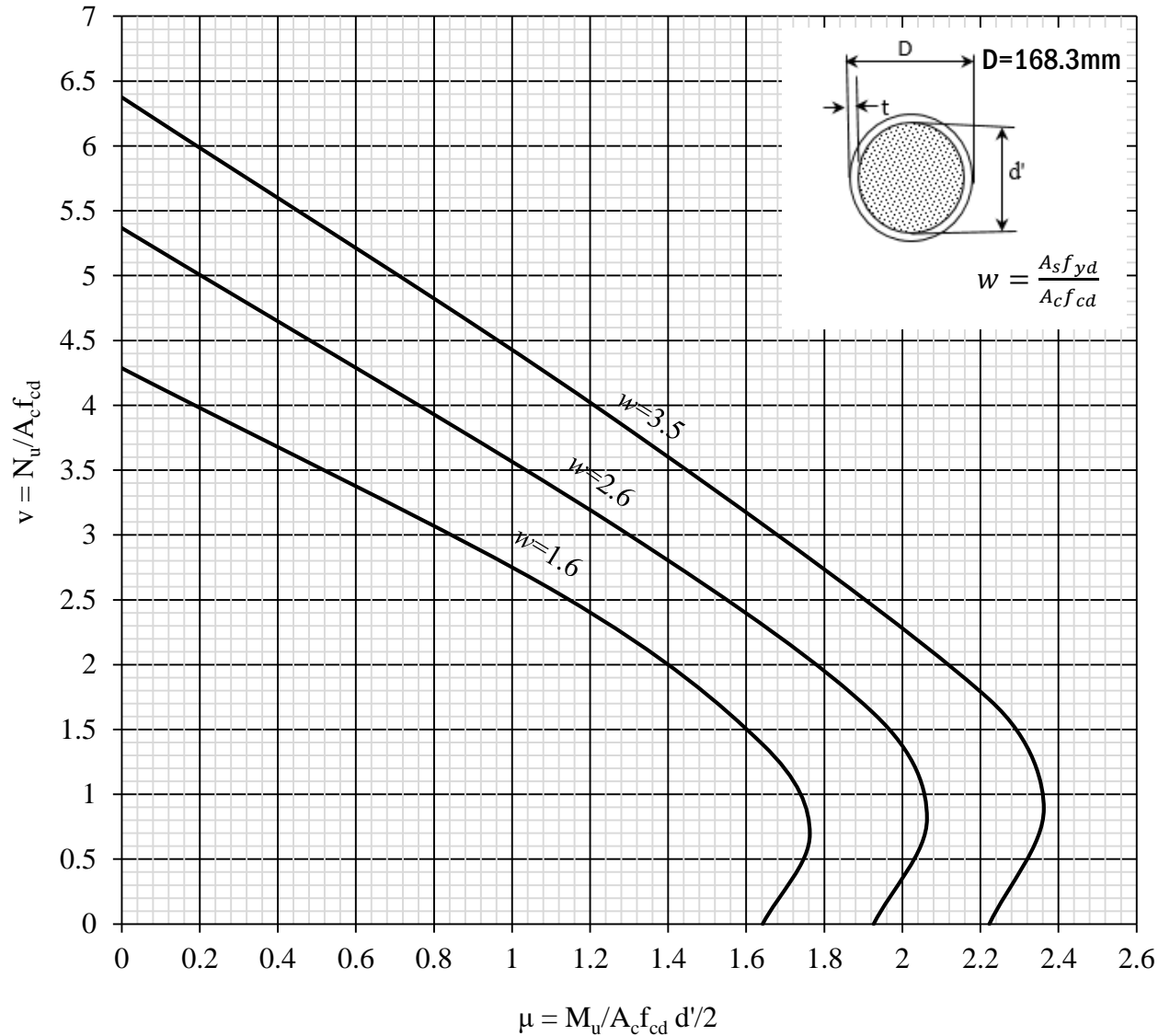
Figure 4.21 Uniaxial Interaction diagram for CCFST with D=168.3mm and varying steel ratios

Uniaxial chart for D=168.3mm and varying steel ratios has been constructed to observe the effect of confinement. As shown in the chart, steel ratio variation influences strength of CCFST column under axial compression. From the interaction curve it has been noted that,

ultimate load capacity of the CCFST columns increases by 48% while value of steel ratio '*w*' rises from 1.6 to 3.5.

4.3.2 Interaction curve for eccentric axial loading condition

Uniaxial interaction diagram for eccentrically axial loading condition is traced to illustrate the effect of non-concentric axial load in determining ultimate strength or capacity of circular concrete infilled steel composite columns.
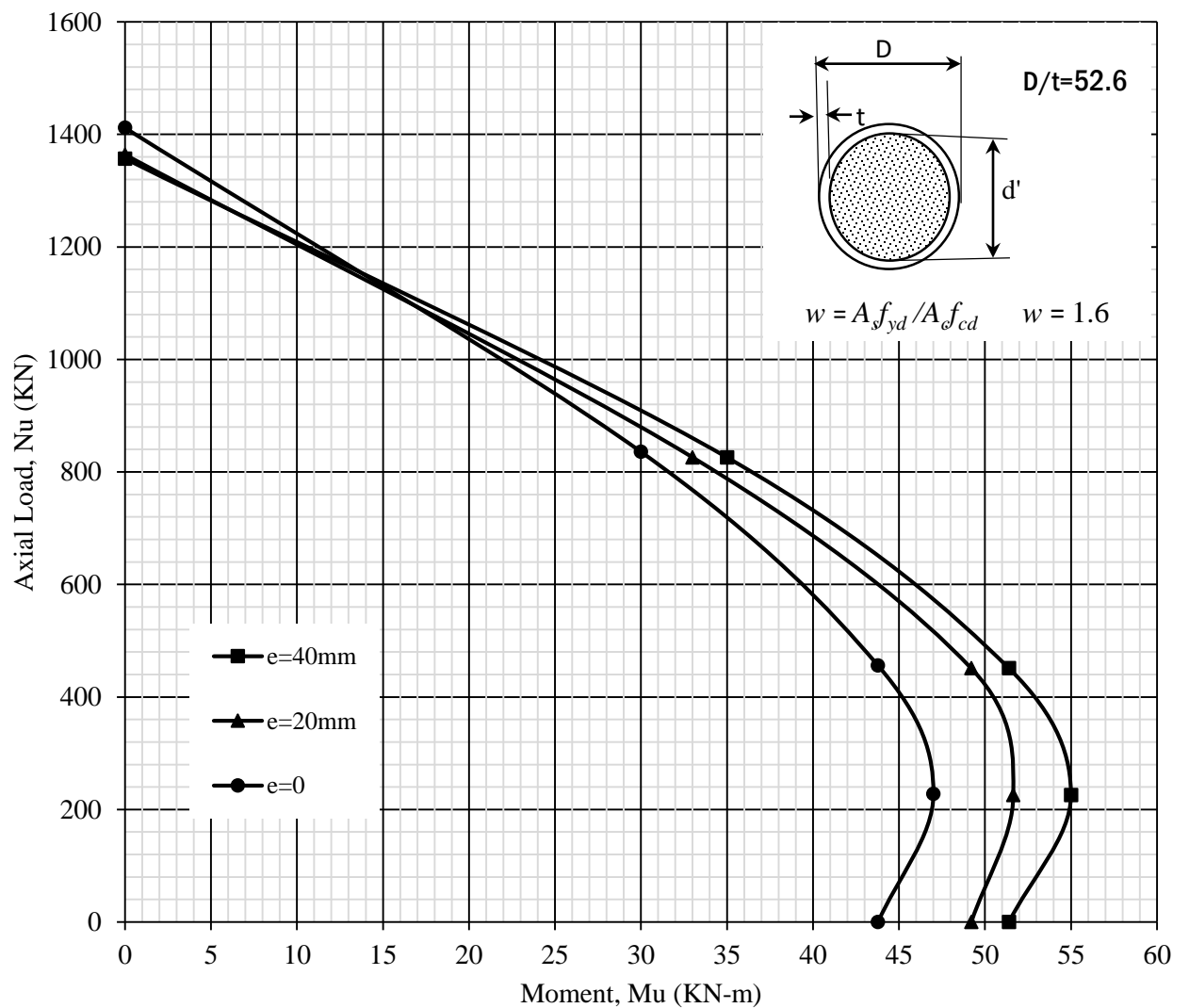
Figure 4.22 N-M interaction curve for eccentric axial loading condition in comparison with concentric loading

4.3.3 Uniaxial interaction charts of normalized axial load and moment capacity for different diameters and thicknesses of CCFSTs
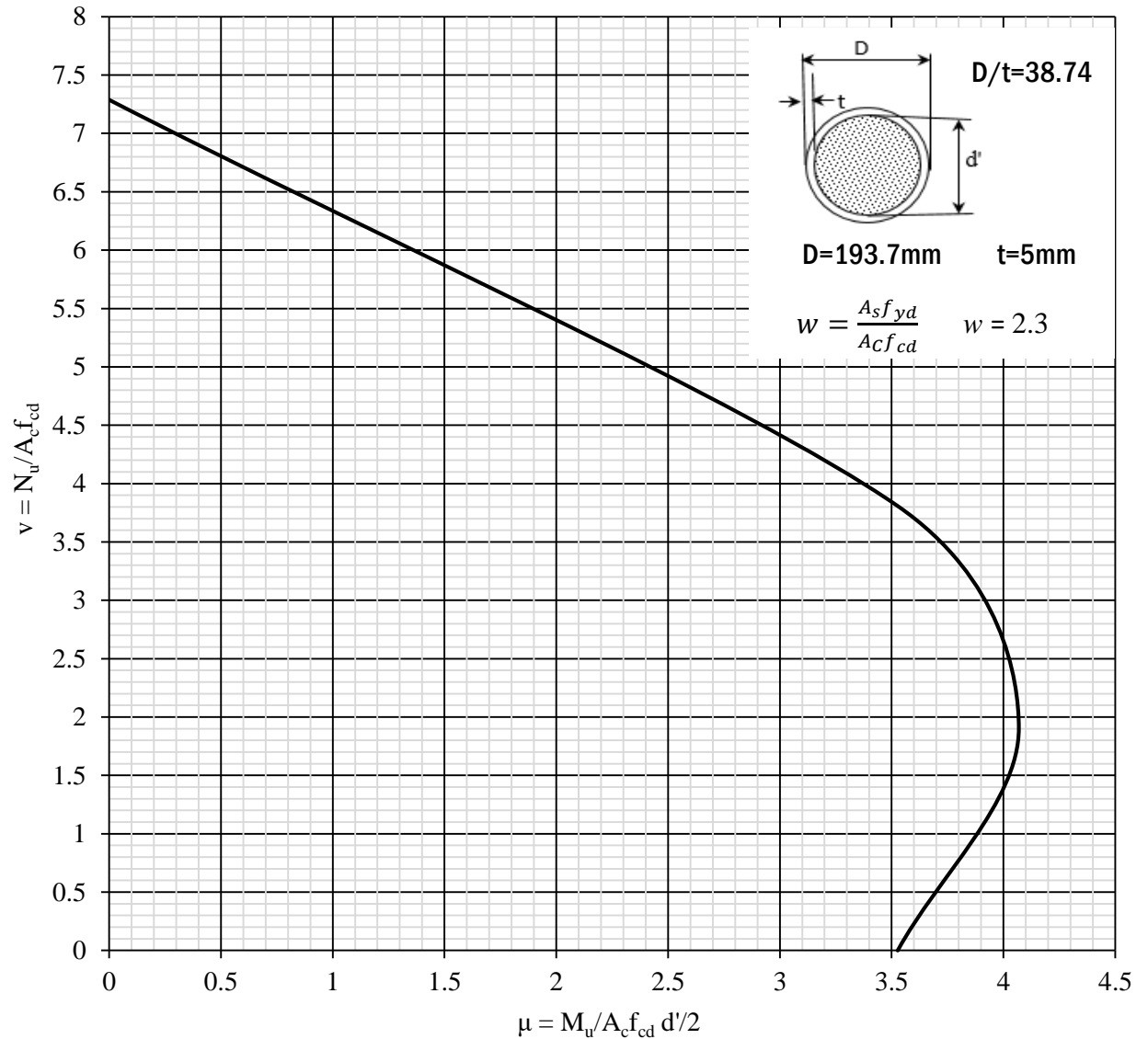
Figure 4.23 Uniaxial interaction chart for D=193.7mm and D/t=38.74

The uniaxial interaction diagrams for varying diameters of CCFST sections shows that strength and ultimate resistance for applied axial load is mainly influenced by increasing cross-sectional area of circular CFST column. While diameter increases from 168.3mm to 193.7mm having similar tube thickness t=5mm, axial load capacity of the section raised by 35%.

Interaction curve for D=244.5mm with varying steel tube thickness is also presented. As steel ratio increases from 2 to 3 moment and load capacity of the section raised by 12% and 23% respectively.
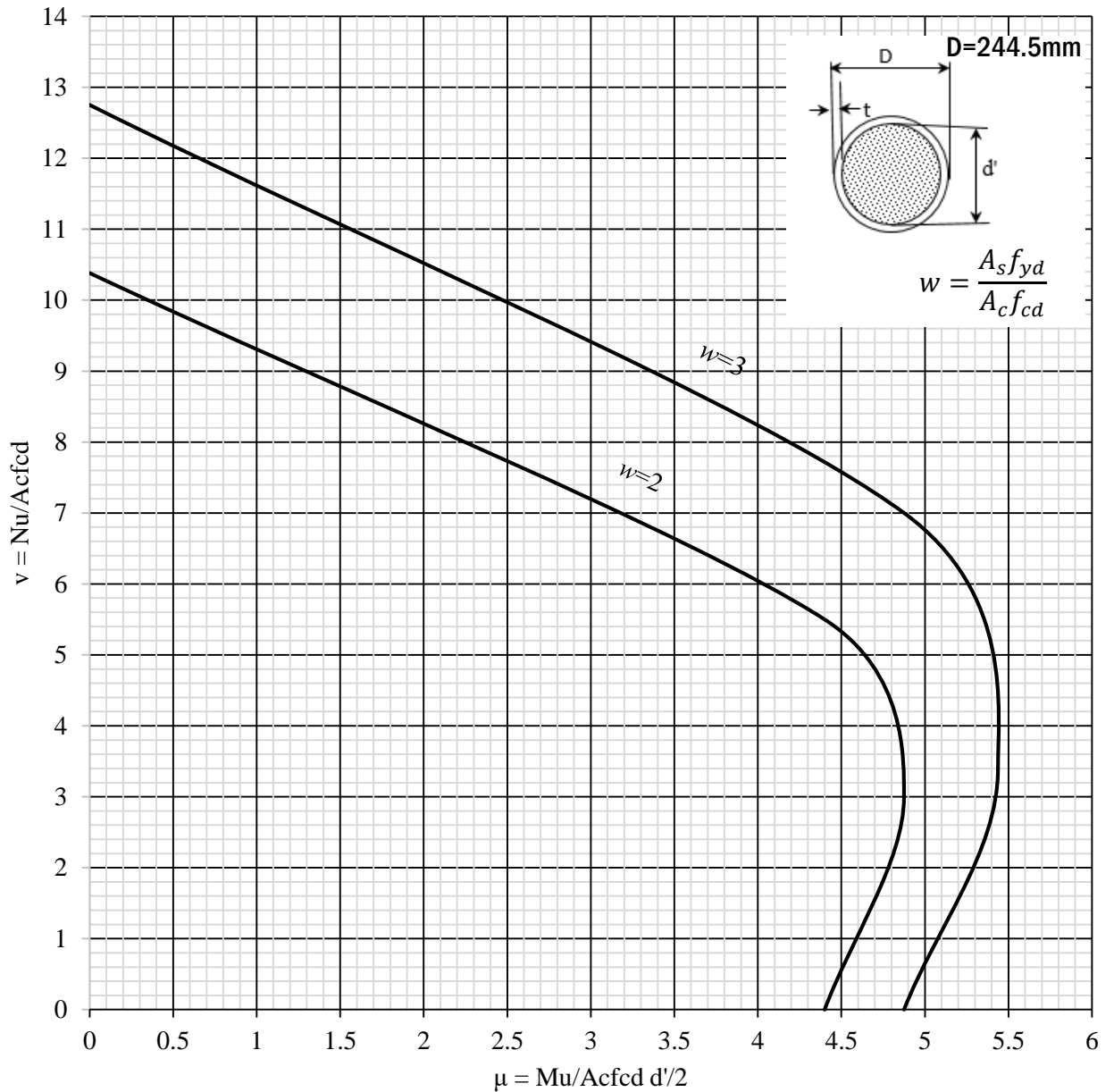
Figure 4.24 Uniaxial Interaction diagram for CCFST with D=244.5mm and varying steel ratios

4.3.4 Comparison of strength interaction curves based on D/t ratio variation
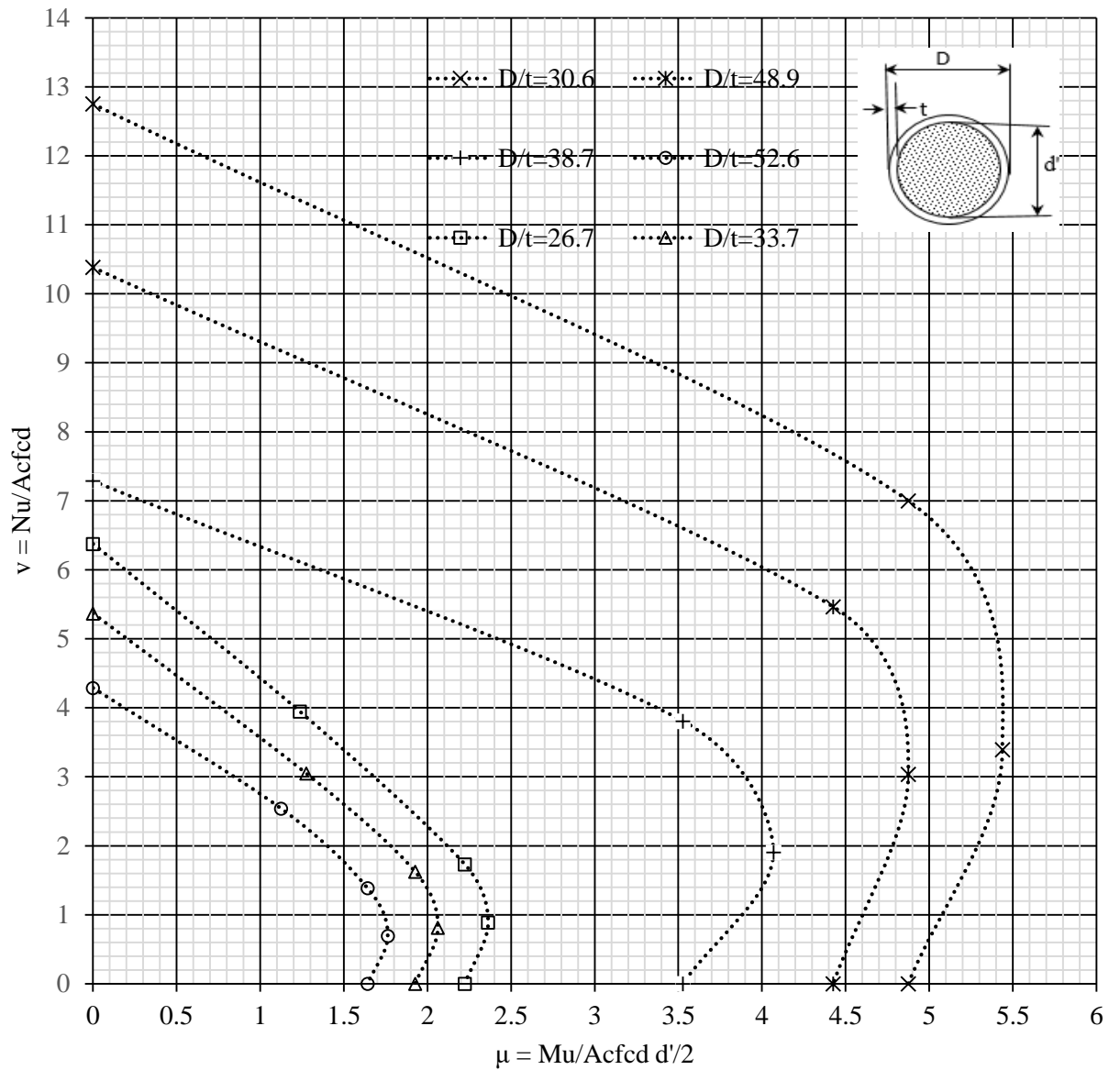
Figure 4.25 Normalized N-M interaction curve comparison for varying D/t ratios

CHAPTER FIVE

CONCLUSIONS AND RECOMMENDATIONS

5.1 Conclusions

Concrete filled steel tube columns in general have significant structural and economic advantages. Particularly, circular hollow steel sections infilled with concrete offer better stiffness, confinement and ductility as compared with square and rectangular CFSTs. However, their design has been difficult and time consuming as it requires rigorous section analysis to construct interaction curves for each trial cross-section. The simplified design procedure that was given in Eurocode 4, follows a trial and error procedure to determine the necessary cross-section for a given load using plastic-stress distribution method. This thesis developed normalized uniaxial charts that simplify the design calculation. In this study, the strength and behavior of CFTs under axial loading was studied. The research approach was as follows. A finite-element model capable of simulating generalized conditions, including the impact of confinement and axial load, was developed using ABAQUS standard/ static general. The study parameters included diameter to thickness ratio (D/t), steel ratio (w), axial load and slenderness ratio. The results from the numerical analysis were further used to compute axial load and moment capacity of the column which are used to develop the N-M interaction diagram. Based on the observations from the developed interaction diagrams the following conclusions are made.

- Higher steel ratio increases strength of CCFST column since larger confinement maximizes axial load and moment capacity by 25% and 17% respectively.
- Smaller D/t ratios provide a significant increase in load and moment capacity as well as being economical sections hence have smaller cross-sectional diameter.
- Compressive resistance of all columns decreases with increase in length of columns. Since the lateral deflection prior to failure increases the bending moment.
- The strength of CFST column predicted by EC4 are found to be conservative. It underestimates the load capacity by 63% as compared with the FE analysis results.

5.2 Recommendations

In this study finite element method was used to simulate the behavior of circular concrete filled steel tube column. Strength of the CCFSTs were also evaluated and N-M uniaxial interaction charts were generated. But this research only covers strength analysis of circular CFST columns with few cross-sectional dimensions having fixed concrete and steel grade, which are under axial load and uniaxial bending. The following recommendations are given for further related researches.

- Uniaxial charts for other Circular CFST cross-sectional dimensions with various steel ratio and D/t values can be generated.
- Strength analysis of CFSTs with internal reinforcement can also be incorporated.
- Interaction curves for CFST columns subjected to axial load and biaxial bending can be developed.
- Influence of concrete and steel strength over the resistance capacity of CFST sections can also be integrated.
- Furthermore, a generic computer program for the analysis of arbitrary CFST sections that enables to plot uniaxial charts can be developed.

REFERENCES

[1] Dundu M. Compressive strength of circular concrete filled steel tube columns. Thin Walled Structures. 2012; 56:62–70.

[2] Dege S. Uniaxial Interaction Charts for Fully Encased Composite Columns. Addis Ababa University, 2015.

[3] EBCS-EN 1994-1-1: 2013: "EBCS 4: Design of composite steel and concrete structures-part 1-1: General rules and rules for buildings", 70-80.

[4] European Committee for Standardization (ECS), Eurocode 4: Design of Composite Steel and Concrete Structures, Part 1-1: General rules and rules for buildings, Brussels, Belgium, 2004.

[5] Chacko, D. and Varghese, M.G. Nonlinear behavior of RCC core steel composite column. International journal of engineering and technology. 2016; 5(07):630-634.

[6] Ketema, E. and Taye, S. Preparation of uniaxial chart for rectangular concrete filled steel columns based on rigid plastic principles. Journal of EEA. 2005; 22.

[7] Johnson, R.P. Composite structures of steel and concrete. 3rd ed. Warwick: Blackwell, 2004.

[8] Bahrami, A., Wan Badaruzzaman, W.H. and Osman, S.A. Behavior of stiffened concrete-filled steel composite (CFSC) stub columns. Latin American Journal of Solids and Structures. 2013; 10:409-439.

[9] Moon, J., Lehman, D., Roeder, W.C. and Lee,H-E. Strength of Circular Concrete Filled Tubes with and without Internal Reinforcement under Combined Loading. Journal of structural engineering. 2013; 139(12).

[10] Giakoumelis G, Lam D. Axial capacity of circular concrete-filled tube columns. Journal of Constructional Steel Research. 2004; 60:1049–68.

[11] Schneider S.P. Axially loaded concrete-filled steel tubes. Journal of structural engineering. 1998;124(10):1125–38.

[12] O'Shea M.D., Bridge R.Q. Design of circular thin-walled concrete filled steel tubes. Journal of structural engineering. 2000;126(11):1295–303.

[13] Ekmekyapar T, Al-eliwi B.J.M. Experimental behaviour of circular concrete filled steel tube columns and design specifications. Thin Walled Structures. 2016; 105:220-30.

[14] Goel, T. and Tiwary, K.A. Finite element modeling of circular concrete filled steel tube (CFST). Indian journal of science and technology. 2018; 11(34).

[15] Ellobody E, Young B, Lam D. Behaviour of normal and high strength concrete-filled compact steel tube circular stub columns. 2006; 62:706–15.

[16] Yonas, T. Y., Temesgen, W. and Senshaw, F. W. Finite element analysis of slender composite column subjected to eccentric loading. International Journal of Applied Engineering Research. 2018; 13(15): 11730-37.

[17] ABAQUS Standard User's Manual. Hibbitt, Karlsson and Sorensen, Inc. Version 6.11, USA; 2011.

[18] Krishan A.L., Astafeva M.A. and Chernyshova E.P. Strength Calculation of Short Concrete-filled Steel Tube Columns. International Journal of Concrete Structures and Materials. 2018; 12:84.

[19] Abbas Y.R. Nomlinear finite element analysis to the circular CFST stub columns. Procedia Engineering. 2017; 173:1692 – 1699.

[20] El-Heweity M.M. On the performance of circular concrete-filled high strength steel columns under axial loading. Alexandria Engineering Journal. 2012;51(2):109–19.

[21] Lianqiong Z, Hang Y. Materials Science and Engineering. Numerical Study on the axial compression performance of concrete-filled steel tubular hybrid columns. 2018;392.

[22] Kwon Y.B., Park S.W. Resistance of circular concrete-filled tubular sections to combined axial compression and bending. Thin Walled Structures. Elsevier; 2017; 111:93–102.

[23] Schnabl S, Jelenić G, Planinc I. Analytical buckling of slender circular concrete-filled steel tubular columns with compliant interfaces. Journal of Constructional Steel Research Analytical. 2015; 115:252–62.

[24] Saleh S.M, Hussain H.K, Bremani A, Hassan A.A. Interaction curves for concrete filled square steel tube columns under axial compression and uniaxial bending. International Conference on Civil and Architectural Engineering. 2017.

[25] Piscesa B, Attard M.M, Suprobo P. Numerical Investigation on The Behavior of Concrete-Filled-Steel-Tube Column under Eccentric Loading. 2017.

[26] Unterweger H, Kettler M. Design of composite columns based on Eurocode Comparison between general and simplified methods. International Conference on Advances in Steel-Concrete Composite Structures. 2018;(Asccs):757–62.

[27] EBCS EN 1992-1-1:2013: EBCS 2: Design of concrete structures.

[28] Ketema, E. Design Aid for Composite Columns (Concrete Filled Tubes). Addis Ababa University, 2005.

APPENDICES

Appendix A: Input file for a reference CCFST model

*Heading

** Job name: D168L2000withplate Model name: Model-1

** Generated by: Abaqus/CAE 2017

*Preprint, echo=NO, model=NO, history=NO, contact=NO

** PARTS

*Part, name="Base Plate"

*Element, type=R3D4

*End Part

*Part, name="Load Plate"

*Element, type=R3D4

*End Part

*Part, name="concrete core"

*Element, type=C3D8R

** Section: concrete

*Solid Section, elset=Set-1, material=C-30

*End Part

*Part, name="steel tube"

*Element, type=C3D8R

** Section: steel

*Solid Section,elset=Set-1, material=S 355 H,

*End Part

** ASSEMBLY

*Assembly, name=Assembly

*Instance, name="steel tube-1", part="steel tube"

*End Instance

*Instance, name="concrete core-1", part="concrete core"

*End Instance

*Instance, name="Base Plate-1", part="Base Plate"

*End Instance

*Instance, name="Load Plate-1", part="Load Plate"

*End Instance

** INTERACTIONS

** Constraint: CP-1-steel tube-1-concrete core-1

*Tie, name="CP-1-steel tube-1-concrete core-1", adjust=yes, type=SURFACE TO SURFACE

"CP-1-concrete core-1", "CP-1-steel tube-1"

** Constraint: CP-2-steel tube-1-concrete core-1

*Tie, name="CP-2-steel tube-1-concrete core-1", adjust=yes, type=SURFACE TO SURFACE

"CP-2-concrete core-1", "CP-2-steel tube-1"

**Constraint: CP-3-Base Plate1-steel tube-1

*Tie, name="CP-3-Base Plate-1-steel tube-1", adjust=yes, type=SURFACE TO SURFACE

"CP-3-steel tube-1", "CP-3-Base Plate-1"

** Constraint: CP-4-Load Plate1-steel tube-1

*Tie, name="CP-4-Load Plate-1-steel tube-1", adjust=yes, type=SURFACE TO SURFACE

"CP-4-steel tube-1", "CP-4-Load Plate-1"

** Constraint: CP-5-Base Plate-1-concrete core-1

*Tie, name="CP-5-Base Plate-1-concrete core-1", adjust=yes, type=SURFACE TO SURFACE

"CP-5-concrete core-1", "CP-5-Base Plate1"

** Constraint: CP-6-Load Plate-1-concrete core-1

*Tie, name="CP-6-Load Plate-1-concrete core-1", adjust=yes, type=SURFACE TO SURFACE

"CP-6-concrete core-1", "CP-6-Load Plate1"

*End Assembly

** MATERIALS

*Material, name=C-30

*Density

 2.4e-09,

*Elastic

30580., 0.2

*Concrete Damaged Plasticity

36.,   0.1, 1.16, 0.667, 1e-05

*Concrete Compression Hardening

   12.,   0.

 20.7149,   0.000178789

 26.4361,   0.000419753

 29.4187,   0.000750246

   30,   0.00102836

 29.8903,   0.00116283

 28.0541,   0.00165086

24.0917,   0.0022084

18.1663,   0.00283011

16.9203,   0.00294684

*Concrete Tension Stiffening,
type=DISPLACEMENT

2.35543,   0.

2.0258,   0.01

1.69617,   0.02

1.36654,   0.03

1.03691,   0.04

0.471085, 0.05

0.465246, 0.06

0.444644, 0.07

0.424043, 0.08

0.403441, 0.09

0.382839, 0.1

0.362237, 0.11

0.341635, 0.12

0.321034, 0.13

0.300432, 0.14

0.27983,   0.15

0.259228, 0.16

0.238627, 0.17

0.218025, 0.18

0.197423, 0.19

0.176821, 0.2

0.156219, 0.21

0.135618, 0.22

0.115016, 0.23

0.0944142, 0.24

0.0738123, 0.25

0.0532106, 0.26

0.0326088, 0.27

*Concrete Compression Damage

0.,   0.

0., 0.000178789

0., 0.000419753

0., 0.000750246

0., 0.00102836

0.00365584, 0.00116283

0.064864, 0.00165086

0.196944,   0.0022084

0.394456, 0.00283011

0.43599, 0.00294684

*Concrete Tension Damage,
type=DISPLACEMENT

0.,   0

0.139944, 0.01

0.279888, 0.02

0.419833, 0.03

0.559777, 0.04	*Material, name=S 355 H
0.8, 0.05	*Density
0.802479, 0.06	7.8e-09,
0.811226, 0.07	*Elastic
0.819972, 0.08	205000., 0.3
0.828719, 0.09	*Plastic
0.837465, 0.1	355., 0.
0.846212, 0.11	355., 0.2
0.854958, 0.12	** BOUNDARY CONDITIONS
0.863705, 0.13	** Name: BOTTOM Type: Displacement/Rotation
0.872451, 0.14	*Boundary
0.881198, 0.15	BOTTOM, 1, 1
0.889944, 0.16	BOTTOM, 2, 2
0.898691, 0.17	BOTTOM, 3, 3
0.907437, 0.18	** Name: TOP Type: Displacement/Rotation
0.916184, 0.19	
0.92493, 0.2	*Boundary
0.933677, 0.21	TOP, 1, 1
0.942423, 0.22	TOP, 2, 2
0.95117, 0.23	** --
0.959916, 0.24	**
0.968663, 0.25	** STEP: Step-1
0.977409, 0.26	*Step, name=Step-1, nlgeom=YES, inc=150
0.986156, 0.27	

*Static

0.01, 1., 1e-05, 1.

**

** BOUNDARY CONDITIONS

** Name: AXIAL LOAD Type: Displacement/Rotation

*Boundary

Loading Set, 3, 3, -100.

** OUTPUT REQUESTS

*Restart, write, frequency=0

** FIELD OUTPUT: F-Output-1

*Output, field

*Node Output

CF, RF, RM, U

*Element Output, directions=YES

DAMAGEC, E, MISES, PEEQ, SF

*Contact Output

CDISP,

** HISTORY OUTPUT: H-Output-1

*Output, history, variable=PRESELECT

*End Step

Appendix B: Calculated values for Concrete damaged plasticity model and steel tube behaviors

Table B- 1 Material input data for steel tube

Material behavior of steel tube	
Density (Kg/m^3)	7800
$Es(Gpa)$	205
Poisson's ratio, n	0.3

Table B- 2 Concrete damaged plasticity model inputs

Concrete damaged plasticity parameters inputs in ABAQUS	
Density (Kg/m^3)	2400
$Ecm\ (Gpa)$	30.58
$fcm\ (Mpa)$	30
ε_{c1}	0.200912
ε_c	3.5
k	2.150961963
$ft\ (Mpa)$	2.355427
$G_f\ (N/m)$	134.649
$Wc\ (mm)$	0.294
c_1	3
c_2	6.9

Table B- 3 Input values for plastic behavior of steel tube

Yield Stress (Mpa)	Plastic Strain
355	0
355	0.2

Table B-4 Compressive behavior of concrete

Strain ε_c	η $\varepsilon_c/\varepsilon_{c1}$	σ_c (Mpa)	$\varepsilon_{elastic}$ σ_c/E_{Cm}	$\varepsilon_{inelastic}$ $\varepsilon_c - \varepsilon_{celastic}$	Damage parameter dc $1\text{-}\sigma_c/f_{Cm}$	$\varepsilon_{plastic}$
0	0	0	0	0	0	0
0.000428	0.213028712	12	0.000392298	3.57021E-05	0	3.57E-05
0.000856	0.426057423	20.71501541	0.000677205	0.000178795	0	0.000179
0.001284	0.639086135	26.43613876	0.000864237	0.000419763	0	0.00042
0.001712	0.852114846	29.41869234	0.000961741	0.000750259	0	0.00075
0.020091	1	30	0.000980745	0.019110444	0	0.01911
0.00214	1.065143558	29.89032795	0.000977159	0.001162841	0.00365573	0.001159
0.002568	1.278172269	28.05414543	0.000917132	0.001650868	0.06486182	0.001587
0.002996	1.491200981	24.09191559	0.000787601	0.002208399	0.19693615	0.002015
0.003424	1.704229693	18.16680848	0.0005939	0.0028301	0.39443972	0.002443
0.0035	1.742057221	16.92084735	0.000553168	0.002946832	0.43597175	0.002519

Table B- 5 Tensile behavior of concrete

Crack displacement			Stress			Damage
w		f(w)	σ/f_t	σ_t	σ_t	$(1-\sigma_t/f_t)$
mm	m			Mpa	Pa	
0	0	1	1	2.355427	2355427.323	0
0.029383133	2.938E-05	0.542071	0.537372	1.265741	1265740.697	0.4626
0.058766265	5.877E-05	0.33877	0.329372	0.775812	775811.7753	0.6706
0.088149398	8.815E-05	0.254245	0.240148	0.56565	565650.4013	0.7599
0.117532531	1.175E-04	0.211733	0.192936	0.454447	454446.9643	0.8071
0.146915663	1.469E-04	0.179229	0.155733	0.366818	366817.6731	0.8443
0.176298796	1.763E-04	0.147728	0.119533	0.281552	281551.9877	0.8805
0.205681929	2.057E-04	0.117109	0.084215	0.198363	198362.8578	0.9158
0.235065062	2.351E-04	0.0893	0.051707	0.121792	121792.4937	0.9483
0.264448194	2.644E-04	0.065764	0.023472	0.055286	55285.65358	0.9765
0.293831327	2.938E-04	0.046991	0	0	0	1

Table B- 6 Input values for compressive behavior of concrete

Yield Stress (Mpa)	Inelastic Strain
12	0
20.7149	0.000178789
26.4361	0.000419753
29.4187	0.000750246
30	0.00102836
29.8903	0.00116283
28.0541	0.00165086
24.0917	0.0022084
18.1663	0.00283011
16.9203	0.00294684

Table B- 7 Inputs for concrete compression damage

Damage Parameter	Inelastic Strain
0	0
0	0.000179
0	0.00042
0	0.00075
0	0.001028
0.003656	0.001163
0.064864	0.001651
0.196944	0.002208
0.394456	0.00283
0.43599	0.002947

Table B-8 Inputs for tensile behavior of concrete

Yield Stress	Displacement
2.35543	0
2.0258	0.01
1.69617	0.02
1.36654	0.03
1.03691	0.04
0.471085	0.05
0.465246	0.06
0.444644	0.07
0.424043	0.08
0.403441	0.09
0.382839	0.1
0.362237	0.11
0.341635	0.12
0.321034	0.13
0.300432	0.14
0.27983	0.15
0.259228	0.16
0.238627	0.17
0.218025	0.18
0.197423	0.19
0.176821	0.2
0.156219	0.21
0.135618	0.22
0.115016	0.23
0.0944142	0.24
0.0738123	0.25
0.0532106	0.26
0.0326088	0.27

Table B- 9 Input values for concrete tension damage

Damage	Displacement
0	0
0.139944	0.01
0.279888	0.02
0.419833	0.03
0.559777	0.04
0.8	0.05
0.802479	0.06
0.811226	0.07
0.819972	0.08
0.828719	0.09
0.837465	0.1
0.846212	0.11
0.854958	0.12
0.863705	0.13
0.872451	0.14
0.881198	0.15
0.889944	0.16
0.898691	0.17
0.907437	0.18
0.916184	0.19
0.92493	0.2
0.933677	0.21
0.942423	0.22
0.95117	0.23
0.959916	0.24
0.968663	0.25
0.977409	0.26
0.986156	0.27

Appendix C: EC-4 method of Axial load and Moment computation for case-II

Table C- 1 EC-4 method of N & M calculation foe case-II

hi	D	d'	(d'/2)^2	(d/2)^2	hi^2	πd'^2/4	2hi/d'	2hi/d	c	c'	d'^3/8	d^3/8	sin c	sin c'
0	168.3	161.9	6552.9025	7081.2225	0	20586.55	0	0	1.57079633	1.57079633	530457.457	595884.873	1	1
5	168.3	161.9	6552.9025	7081.2225	25	20586.55	0.06176652	0.05941771	1.5113436	1.50899046	530457.457	595884.873	0.99823321	0.99809063
10	168.3	161.9	6552.9025	7081.2225	100	20586.55	0.12353305	0.11883541	1.45167943	1.44694691	530457.457	595884.873	0.99291397	0.99234046
15	168.3	161.9	6552.9025	7081.2225	225	20586.55	0.18529957	0.17825312	1.39158547	1.38441963	530457.457	595884.873	0.98398467	0.98268208
20	168.3	161.9	6552.9025	7081.2225	400	20586.55	0.24706609	0.23767083	1.33082907	1.32114502	530457.457	595884.873	0.97134576	0.96899863
25	168.3	161.9	6552.9025	7081.2225	625	20586.55	0.30883261	0.29708853	1.26915426	1.25683093	530457.457	595884.873	0.95484994	0.95111641
30	168.3	161.9	6552.9025	7081.2225	900	20586.55	0.37059914	0.35650624	1.20627058	1.19114232	530457.457	595884.873	0.93429294	0.92879292
35	168.3	161.9	6552.9025	7081.2225	1225	20586.55	0.43236566	0.41592395	1.14183776	1.12368164	530457.457	595884.873	0.9093994	0.90169836
40	168.3	161.9	6552.9025	7081.2225	1600	20586.55	0.49413218	0.47534165	1.07544401	1.05395998	530457.457	595884.873	0.87980129	0.86938679
45	168.3	161.9	6552.9025	7081.2225	2025	20586.55	0.5558987	0.53475936	1.00657339	0.9813526	530457.457	595884.873	0.8450044	0.83125004
50	168.3	161.9	6552.9025	7081.2225	2500	20586.55	0.61766523	0.59417706	0.93455419	0.90502588	530457.457	595884.873	0.80433427	0.78644114
55	168.3	161.9	6552.9025	7081.2225	3025	20586.55	0.67943175	0.65359477	0.85847189	0.82380843	530457.457	595884.873	0.75684468	0.73373871
60	168.3	161.9	6552.9025	7081.2225	3600	20586.55	0.74119827	0.71301248	0.77701098	0.73594269	530457.457	595884.873	0.70115134	0.67128617
65	168.3	161.9	6552.9025	7081.2225	4225	20586.55	0.80296479	0.77243018	0.68813757	0.63854338	530457.457	595884.873	0.63509969	0.59602646
70	168.3	161.9	6552.9025	7081.2225	4900	20586.55	0.86473132	0.83184789	0.58836739	0.52618118	530457.457	595884.873	0.55500368	0.50223476
75	168.3	161.9	6552.9025	7081.2225	5625	20586.55	0.92649784	0.8912656	0.47066792	0.3857996	530457.457	595884.873	0.45348168	0.37630009
80	168.3	161.9	6552.9025	7081.2225	6400	20586.55	0.98826436	0.9506833	0.31536477	0.15335361	530457.457	595884.873	0.31016327	0.15275324
80.95	168.3	161.9	6552.9025	7081.2225	6552.9025	20586.55	1	0.96197267	0.2766616	0	530457.457	595884.873	0.27314572	0

hi^3	tan c'	tan c	Wseg,C	Wseg,T	Wseg, a	Mu	Mu (KNm)	Acc	Asnet	Nu	Nu (KN)	v	μ
0	1.63246E+16	1.63246E+16	353638.305	397256.582	43618.3	33811804.46	33.81180446	10293.2748	0	164692.397	164.7	0.50	1.27
125	16.15908723	16.80026488	354309.668	395154.69	40845.0	32032537.89	32.03253789	11102.2598	64.042981	198304.556	198.3	0.60	1.20
1000	8.032996016	8.355371027	356284.929	388871.361	32586.4	26733602.3	26.7336023	11908.1476	128.319033	231942.378	231.9	0.70	1.00
3375	5.303207625	5.520153983	359446.242	378474.039	19027.8	18032707.73	18.03270773	12707.8049	193.076771	265635.965	265.6	0.81	0.68
8000	3.922021959	4.08693727	363592.484	364076.497	484.0	6129887.728	6.129887728	13498.0243	258.577824	299418.434	299.4	0.91	0.23
15625	3.079714922	3.214024891	368431.557	345840.997	-22590.6	-8686262.614	-8.686262614	14275.4813	325.111065	333329.82	333.3	1.01	-0.33
27000	2.506192885	2.620691703	373568.224	323981.57	-49586.7	-26028812.61	-26.02881261	15036.6841	393.006039	367420.606	367.4	1.12	-0.98
42875	2.0854995	2.18645599	378485.608	298768.698	-79716.9	-45397828.83	-45.39782883	15777.9107	462.651281	401756.631	401.8	1.22	-1.70
64000	1.759421514	1.850881969	382517.122	270535.89	-111981.2	-66158459.56	-66.15845956	16495.1275	534.520775	436426.326	436.4	1.32	-2.48
91125	1.495326464	1.58015822	384802.938	239688.946	-145114.0	-87507559.65	-87.50755965	17183.8782	609.214253	471551.939	471.6	1.43	-3.28
125000	1.273248208	1.353694574	384219.73	206719.201	-177500.5	-108420910.3	-108.4209103	17839.1242	687.522228	507307.972	507.3	1.54	-4.07
166375	1.079929979	1.157972366	379260.348	172223.097	-207037.3	-127564856.3	-127.5648563	18455.0019	770.538139	543953.492	544.0	1.65	-4.78
216000	0.905676926	0.983364759	367809.981	136932.461	-230877.5	-143135859.1	-143.1358591	19024.4263	859.868516	581893.607	581.9	1.77	-5.37
274625	0.742282184	0.822209824	346677.283	101764.615	-244912.7	-152533024.8	-152.5330248	19538.3797	958.073135	621810.144	621.8	1.89	-5.72
343000	0.580798623	0.667193712	310418.734	67913.9037	-242504.8	-151559012.7	-151.5590127	19984.4493	1069.74897	664988.064	665.0	2.02	-5.68
421875	0.406153228	0.508806447	247304.72	37046.7698	-210258.0	-131754959.7	-131.7549597	20343.0547	1205.02454	714382.829	714.4	2.17	-4.94
512000	0.154567188	0.326252993	106778.332	11853.3803	-94925.0	-59561236.21	-59.56123621	20570.8687	1400.83466	781221.066	781.2	2.37	-2.23
530457.457	0	0.283943331	0	8095.69836	8095.7	5225400.89	5.22540089	20586.55	1462.87128	801492.861	801.5	2.43	0.20